Geothermics 91 (2021) 102003

Contents lists available at ScienceDirect

Geothermics

journal homepage: www.elsevier.com/locate/geothermics

Sulphur isotopes in deep groundwater reservoirs: Evidence from post-stimulation flowback at the Pohang geothermal facility, Korea

David Banks [a,*], Adrian J. Boyce [a,b], Rob Westaway [a], Neil M. Burnside [a,c]

[a] James Watt School of Engineering, University of Glasgow, James Watt Building South, Glasgow, G12 8QQ, UK
[b] Scottish Universities Environmental Research Centre (SUERC), East Kilbride, G75 0QF, UK
[c] Currently at Department of Civil and Environmental Engineering, University of Strathclyde, James Weir Building, 75 Montrose Street, Glasgow, G1 1XJ, UK

ARTICLE INFO

Keywords:
Pohang
Hydraulic stimulation
Sulphate
34-sulphur
Flowback
Anhydrite

ABSTRACT

A hydraulic stimulation was carried out on a granodiorite reservoir in an enhanced geothermal system in August 2017 in Pohang, Korea. Water injected into the 4.2 km deep PX-1 well contained c. 330−360 mg/L sulphate, with a negative $\delta^{34}S$. The resulting flowback water became more saline with time, with sulphate and chloride concentrations and dissolved sulphate $\delta^{34}S$ all increasing. Compared with conservative advective-dispersive and mixing models, the flowback contained surplus sulphate with an elevated $\delta^{34}S$. The PX-1 reservoir fluid is saturated with respect to anhydrite at downhole temperatures and pressures. Dissolution by injected surface water of secondary anhydrite along fracture surfaces, most likely with elevated $\delta^{34}S$ reflecting the reservoir fluid, is likely to have resulted in an excess of ^{34}S-enriched sulphate in the flowback fluid. An alternative hypothesis involving oxidation of pyrite is also plausible but is stoichiometrically inadequate to account for the observed sulphate excess, and unlikely from a sulphur isotopic perspective. This analysis thus contributes to the evidence for water-rock reactions during stimulation of the Pohang granodiorite.

1. Introduction

The Pohang geothermal site (129°22′46.08″E, 36°06′23.34″N) is located c. 6 km north of the city of Pohang, on the east coast of the Korean peninsula (Fig. 1). Two 4.2 km deep wells have been drilled into a concealed granodiorite below the site, with the intention of creating an enhanced geothermal system (EGS). Five episodes of hydraulic stimulation have been applied to the wells to enhance their hydraulic performance and to achieve acceptable mutual connectivity.

It is widely observed that, in hydraulic stimulation operations, the chemistry of flowback fluid is often significantly different from that of the injected water. The flowback fluid can often be hypersaline, contain excess concentrations of cations (Sr^{2+}, Ba^{2+}, Ca^{2+}) contributing to scale-forming minerals and may also contain naturally occurring radioactive solutes (e.g. radium (Haluszczak et al., 2013)). Most of the published studies of the chemistry of flowback fluid come from the hydrocarbon sector, especially from the hydraulic fracturing of deep organic shales to produce "shale gas". Most of these studies conclude that the dominant factor determining flowback chemistry is mixing between the injected water and a deep, connate, highly reducing brine, potentially of considerable age (Haluszczak et al., 2013; Zolfaghari et al., 2015; Balashov et al., 2015; Vazquez et al., 2014). One recent study (Owen et al., 2020), from the shaly Montney Formation of Canada, considered potential water-rock interaction and proposed a component of ion exchange and possible carbonate dissolution, superimposed on a dominant mixing trend, to account for the flowback chemistry. The study also found an early excess of sulphate in the flowback water, which the authors ascribed (albeit speculatively) to pyrite oxidation.

Similar examples of post-stimulation flowback hydrochemistry from geothermal prospects in other lithologies are scarce. However, a recent study (Burnside et al., 2019) documented the flowback chemistry from one of the deep boreholes in the Pohang granodiorite. It concluded that the dominant process was also mixing between fresh injected water and a saline formation water (though less saline, less reducing and more sulphate-rich than typical shale brines). The study found evidence of water-rock interaction (quartz dissolution and aluminosilicate hydrolysis) and an early excess of sulphate, which was also initially (Burnside et al., 2019) ascribed to sulphide oxidation.

The present study considers the sulphate chemistry and sulphur isotope systematics of this flowback water in more detail and seeks to explain the source of the sulphate excess. Dissolved sulphate is not regarded as a conservative tracer, as it is affected by a range of mineral

* Corresponding author.
E-mail address: David.banks@glasgow.ac.uk (D. Banks).

https://doi.org/10.1016/j.geothermics.2020.102003
Received 1 June 2020; Received in revised form 10 September 2020; Accepted 12 November 2020
Available online 24 December 2020

dissolution and precipitation reactions (gypsum/anhydrite, barite, celestite, pyrite) and is also redox-sensitive, being reduced to sulphide in strongly reducing environments (Miao et al., 2013).

Determination of dissolved sulphate sulphur isotopic composition can be valuable in identifying sources of sulphate (Seal, 2006). In particular, the ratio between ^{34}S (natural abundance 4.21 %) and ^{32}S (natural abundance 95.02 %), expressed as $\delta^{34}S$, is important (Böttcher, 2011). In the context of groundwater, very little isotopic fractionation occurs when sulphate is released to the dissolved phase by dissolution of sulphate salts or oxidation of pyrite and other sulphide minerals (Seal, 2006; Taylor et al., 1984). Dissolved sulphate $\delta^{34}S$ in such cases thus reflects, and potentially identifies, the source mineral (Seal, 2006). However, an important isotopic fractionation occurs when sulphate is reduced to sulphide, especially when microbially facilitated, leaving the sulphide formed depleted in ^{34}S, and the residual fluid enriched.

$$2CH_2O + SO_4^{2-} = H_2S + 2HCO_3^- \text{ where } CH_2O \text{ is generic organic matter} \quad (1)$$

Fractionations of down to -70‰ have been observed experimentally and in the field (Böttcher, 2011; Rye et al., 1981). Large fractionations are typical of situations where the net rate of reduction is low compared to the overall redox turnover of sulphur (Bottrell et al., 2000). The H_2S produced will often be partially immobilised in metal sulphide minerals. Another important fractionation mechanism is that of disproportionation, for example of magmatic SO_2 (Kusakabe et al., 2000; Rye, 2005), to form a sulphate phase enriched in ^{34}S and a depleted sulphide phase (Bayon and Ferrer, 2005):

$$4SO_2 + 4H_2O = 3HSO_4^- + 3H^+ + H_2S \quad (2)$$

The importance of this research, based on the flowback water from Pohang, is two-fold. First, sulphate minerals can be important scale-forming minerals in geothermal systems, especially anhydrite (in higher temperature systems (Zarrouk and McLean, 2019)) and gypsum (Brehme et al., 2019). The solubility of both is very sensitive to calcium and sulphate concentrations and to temperature (anhydrite becomes less soluble with increasing temperature; gypsum has a solubility maximum at 35−40 °C (Rolnick, 1954)). An understanding of sources of excess sulphate in geothermal systems will aid in mitigating scale formation. Second, at the Pohang site, an official study concluded that hydraulic stimulation had contributed to the occurrence of a M_w 5.5 earthquake (GSK, 2019). Mineral dissolution within the stressed fault zone has been postulated as a contributory factor to seismic shear (Westaway and Burnside, 2019; Westaway et al., 2020). A clearer documentation of evidence of water-rock interaction during this hydraulic stimulation is thus timely and essential for further evaluation of this scenario.

2. Background: sulphur in granitoid environments

Section 2 provides a brief review of the occurrence of sulphur in granitoid rocks and their groundwaters, and provides a necessary background for understanding and interpreting the experimental data.

2.1. Sulphur in granitic rocks

Sulphur can exist in igneous rocks in several solid phases. It may be present in its oxidised form as a number of secondary sulphate minerals, including barite ($BaSO_4$) and the calcium sulphates, gypsum ($CaSO_4.2H_2O$, stable at low temperature) and anhydrite ($CaSO_4$, more stable at higher temperature (Van Driessche et al., 2017)). Gypsum has, for example, been observed at depths of down to 1 km in Precambrian granitoids in the Laxemar-Simpewarp area of eastern Sweden (Drake and Tullborg, 2009). Anhydrite is abundant through disproportionation reactions (eqn. 2) in potassic alteration zones of major porphyry mineralising systems (Richards, 2011). Anhydrite is reported (Vidal et al., 2018) as a common mineral within an altered fault plane in a c. 2.5 km deep granite geothermal reservoir at Rittershoffen, France. It is also documented as an alteration product (Savage et al., 1987) at elevated temperature in the Cornish Carnmenellis granite, UK. Secondary anhydrite is reported (Muramatsu et al., 2000) from several Japanese geothermal systems, including that associated with the Quaternary Kakkonda granite of NE Japan. The presence of considerable readily-soluble $CaSO_4$ in granites and gneisses from the Black Forest of Germany has been demonstrated by leaching experiments (Bucher and

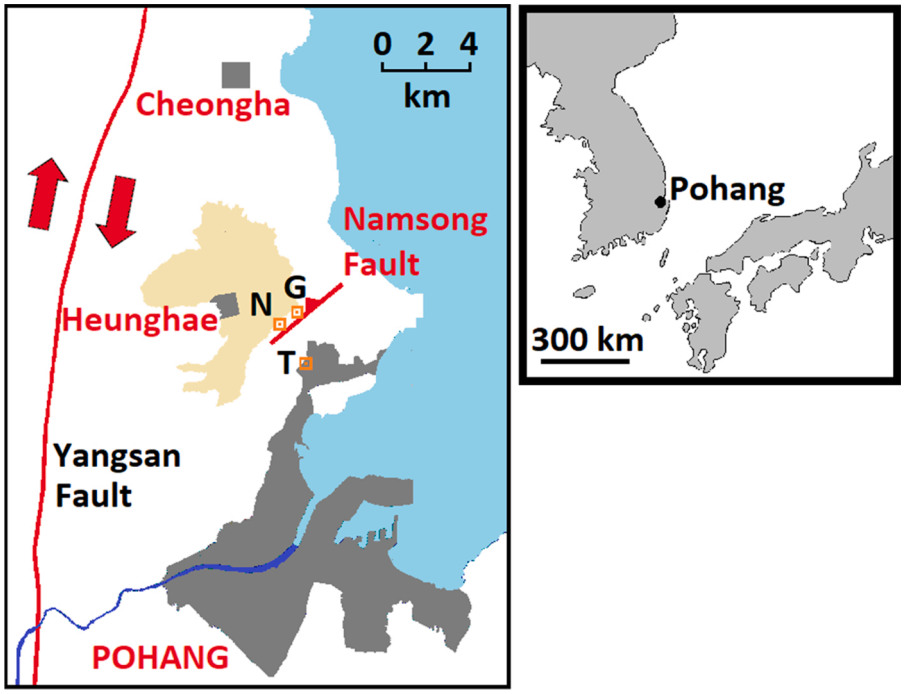

Fig. 1. Location map of Pohang site, showing Pohang city, the Heunghae alluvial plain (pale yellow), the Pohang geothermal site (G), Namsong village (N), and a thermal spa resort in Pohang (T). Modified after (Westaway and Burnside, 2019). (For interpretation of the references to colour in the Figure, the reader is referred to the web version of this article).

Stober, 2010). In non-granitic environments, anhydrite is also reported from several Icelandic geothermal systems including Krafla (volcanic) (Gudmundsson and Arnórsson, 2002) and Grimsey (sediment-hosted) (Kuhn et al., 2003).

The sulphur isotopic composition of such sulphates typically reflects that of the fluid from which they were precipitated (Drake and Tullborg, 2009). For example, the Kakkonda anhydrites exhibited $\delta^{34}S$ values in the range +21.6 to +24.2‰, suggesting (Muramatsu et al., 2000) that the ultimate source of the sulphate was either marine water or Miocene sulphate evaporites.

Alternatively, sulphur may be present in its reduced state as sulphide minerals, which can be primary (lower crustal-mantle-derived magmatic) or hydrothermal in origin, or secondary precipitates (derived from dissolved sulphate in ground water / pore fluids). Primary / hydrothermal pyrite in granitic rocks typically has a $\delta^{34}S$ of around or slightly above 0‰ (Koh et al., 2000; Seal, 2006; Laouar et al., 1990; Kohut and Recio, 2002) (albeit somewhat higher in S-type granites). For example, early stage hydrothermal pyrite (related to a nearby 1.45 Ga granite intrusion) in granitic rocks in Laxemar-Simpewarp (Sweden) exhibited $\delta^{34}S$ of -3 to +3‰ (Drake and Tullborg, 2009); in Korea, primary granite pyrite has shown $d^{34}S$ of +1.8 to +2.6‰ (Park et al., 1991). The formation of secondary sulphides from dissolved sulphate in fluids is widely documented. At low temperatures of up to 60−80 °C, sulphide minerals are typically formed by bacterial sulphate reduction (BSR (Machel, 2001)). This process results in large fractionations, with the sulphide initially formed depleted in ^{34}S (low $\delta^{34}S$), leaving the residual fluid with an elevated $\delta^{34}S$. As sulphide formation progresses in a closed system, the $\delta^{34}S$ of the sulphide increases sharply as ^{34}S becomes enriched in the parent fluid. Thus, in systems that are "open" with respect to sulphate, secondary pyrite produced by BSR typically have $\delta^{34}S$ significantly lower that the parent fluid's sulphate (Seal, 2006). In closed systems, however, late stage secondary sulphides can form with high $\delta^{34}S$, often as ^{34}S-enriched zones around a core depleted in ^{34}S. This was demonstrated in the Precambrian Laxemar granitoids (Drake et al., 2012) where pyrite was found as secondary fracture mineralisation down to 1 km depth, with bulk grain $\delta^{34}S$ ranging from -42 to +54‰ and zonation within the crystals, with the highest $\delta^{34}S$ in the outermost zones. The pyrite was interpreted as derived from BSR of sulphate in the groundwater, with progressive S-isotopic fractionation (Drake et al., 2013).

Although sulphate reducing bacteria (SRB) have been identified that can survive to 110 °C (Machel, 2001), the understood limit for microbial life is currently 122 °C (Takai et al., 2008). At temperatures above 140−160 °C (as at Pohang), sulphate reduction processes are abiotic and are termed thermochemical sulphate reduction (TSR). TSR typically requires a source of carbon (often hydrocarbons (Li et al., 2019; Jia et al., 2015), but potentially other organic compounds, such as carboxylic acids (Kiyosu and Krouse, 1990)), although TSR using alternative electron donors is possible. TSR by ammonium has been inferred to be geologically plausible at temperatures of 50–60 °C (Ding, 2015) and TSR by Fe(II) in, for example, olivine, has also been demonstrated (Seal, 2006). TSR is subject to kinetic fractionations in the range -10 to -20‰, and typically -15‰ at 150 °C (Machel, 2001; Kiyosu and Krouse, 1990). In many natural situations, relatively little TSR fractionation is observed, with the sulphide mineral having a similar isotopic composition to the parent sulphate (Machel, 2001; Li et al., 2019; Jia et al., 2015; Machel et al., 1995), probably due to the kinetics determining initial sulphate mineral dissolution (Cross and Bottrell, 2000).

2.2. Sulphate in granitoid groundwaters

In deep crystalline rock groundwaters, sodium-chloride salinity increases with depth, and water-rock interaction elevates the Ca/Na ratio (Bucher and Stober, 2010; Bottomley et al., 1994; Stober and Bucher, 1999; Brady et al., 2019). The sulphate content of deep granite groundwaters is, however, variable and a simple explanation for its origin and behaviour remains elusive in many cases (Fontes et al., 1989). Sulphate could conceivably be derived from one or more of the following sources:

- Modern infiltration of seawater or inundation in the geological past (Stober and Bucher, 1999; Aquilina et al., 2013). Modern seawater has a $\delta^{34}S$ of +20.6‰ (Tostevin et al., 2014) and a molar SO_4^{2-}/Cl-ratio of 0.052 (Stanford University, 2019).
- Dissolution of evaporite minerals from overlying sedimentary rocks, infiltration of evaporitic brines (Bottomley et al., 1994), or, conceivably, dissolution of secondary sulphate minerals within the granite. Evaporite and secondary sulphate minerals typically have a $\delta^{34}S$ closely corresponding to the seawater / brine from which they were derived (Strauss, 1997).
- Oxidation of pyrite / sulphide fracture minerals. The oxidation of sulphide minerals to aqueous sulphate is accompanied by negligible fractionation (Seal, 2006; Taylor et al., 1984).
- Disproportionation of magmatic SO_2 (Bayon and Ferrer, 2005).

These hypotheses are very similar to those proposed for sulphate in the Stripa granite, Sweden (Fontes et al., 1989). Multiple sources are often invoked to explain the range of observed sulphate $\delta^{34}S$ in deep groundwater reservoirs. For example, at Stripa, three different sulphate processes were hypothesised for groundwater down to 822 m: (i) atmospheric sulphate and sulphide oxidation (characterised by low $\delta^{34}S$) in the shallowest waters, (ii) BSR, reducing the sulphate concentrations and elevating $\delta^{34}S$, in intermediate waters, (iii) an unknown sulphate source in the deepest waters, again progressively modified by sulphate reduction (Fontes et al., 1989). In the upper 400 m of the Laxemar granitoids, high dissolved sulphate $\delta^{34}S$ (+25 to +37‰), coupled with low sulphate concentrations, was explained by the formation of secondary pyrite by BSR. In the same granitoids, a higher dissolved sulphate concentration, with lower $\delta^{34}S$ (+9 to +20‰), at greater depths (400–700 m) was explained by dissolution of fracture-bound Palaeozoic gypsum (Drake et al., 2012, 2013). Both sulphide oxidation and anhydrite dissolution have invoked as sulphate sources in deep Alpine granitic and gneissic rocks (Bucher and Stober, 2010).

It has also been suggested (Banks et al., 2020) that deep groundwater is a dissolved sulphate reservoir whose $\delta^{34}S$ reflects a dynamic equilibrium between various inputs (pyrite oxidation, marine water, secondary sulphate dissolution) and sinks (precipitation of sulphates with little fractionation, formation of sulphides by BSR or TSR, with accompanying fractionation). As sulphide formation progressively dominates, sulphate concentrations become depleted in the reservoir, and residual dissolved sulphate $\delta^{34}S$ increases. In essence, this is exactly the same model that is proposed for the ocean, with relative rates of inputs and outputs controlling marine sulphate $\delta^{34}S$ through geological time (Fike et al., 2015).

Finally, the possibility of S isotope exchange between groundwater sulphate and mineral phases must be considered. While this is geologically slow at low temperatures, rapid equilibration can take place at temperatures > 350 °C, especially at low pH (Seal, 2006). Some degree of isotopic exchange cannot be excluded at lower temperatures, although circumneutral to alkaline pH conditions would be expected to retard the process.

3. The study site

3.1. Granodiorite mineralogy

At the Pohang geothermal site, a cover of c. 2356 m (Miocene marine sediments of the Heunghae Basin, Palaeogene and Cretaceous subduction-related volcanic and sedimentary rocks (Park et al., 2015; Westaway and Burnside, 2019)), overlies a Permian granodiorite, which hosts the target zone for the Pohang Enhanced Geothermal System (EGS) project. The granodiorite comprises quartz, plagioclase, microcline, hornblende, biotite (Lee et al., 2011; Kwon et al., 2019) intruded with

mafic gabbro and amphibolite dykes (Lee et al., 2014; Kim et al., 2018). Chlorite, laumontite (a zeolite: $Ca(AlSi_2O_6)_2{\cdot}4H_2O$) and calcite have also been identified. Anhydrite has not been specifically reported from the Pohang granodiorite, although "gypsum" was detected as a trace fracture mineral at c. 3500–3800 m depth (Table 1, (GSK, 2019)). Pyrite (and other sulphides) are widespread in granitoids of the region around Pohang, as a result of magmatic-hydrothermal activity in the late Cretaceous (Koh et al., 2000; Jo and Shin, 2015).

The unconformity at the top of the granodiorite indicates that it was exhumed and eroded during the Mesozoic, prior to burial by subduction-related volcanics in the Late Cretaceous. This phase of magmatism was accompanied by large-scale regional secondary mineralization (Koh et al., 2003; Yoon and Jung, 2008), producing hydrothermal clays, quartz, Au, Ag and Cu-, Zn- and Pb-sulphides, pyrite and alunite. The $\delta^{34}S$ of this hydrothermal pyrite ranges from around -10 to +10‰, with the lower values (around or below 0‰) indicating a magmatic origin, and the more positive values suggesting some contamination by sedimentary rocks (Koh et al., 2000). The values are broadly similar to regional granite-related ores, which exhibit a strong mode around c. + 4 to +5‰ (Ishihara et al., 2000). Galena and sphalerite exhibit a similar, occasionally slightly higher, $\delta^{34}S$ range (Jo and Shin, 2015; Choi et al., 2018). Alunites (a hydroxysulphate) exhibit a $\delta^{34}S$ range from +3.9 to +16.5‰, but most fall within +5.2 to +8.6‰ (Yoon and Jung, 2008). No pyrite, sulphides or alunite have been documented from granodiorite samples recovered from the deep EGS site boreholes.

3.2. Geothermometry

In the region surrounding the EGS site, temperatures in excess of 90 °C have been recorded at 2000 m depth (Lee et al., 2015) and 103 °C at 2250 m depth (Yoon et al., 2015). Based on calculated geothermal gradients, a temperature of 160 °C has been inferred at 4.3 km depth (Kim and Lee, 2007). Thus, the top of the Pohang granodiorite, at 2356 m depth, is currently at c. 110 °C. Given that it was likely exposed to ambient surface temperatures of c. 30 °C in the Mesozoic, each point within this granodiorite was likely to have been c. 80 °C cooler than at present.

3.3. Drilled wells

At the geothermal site, two deep wells (PX-1 and PX-2) have been drilled to depths of c. 4.2 km in the granodiorite. These were intended to be operated as an Enhanced Geothermal System (EGS), with one borehole used for production of hot fluid and the second for reinjection.

The PX-1 well was initially constructed as a vertical borehole in 2012−13 and then side-tracked in 2016, completed as a deviated well (Fig. 2), with a measured depth of 4362 m and true vertical depth (TVD) of 4215 m (Yoon et al., 2015; Hofmann et al., 2019). The lowermost open hole section is 313 m long and 216 mm in diameter (Hofmann et al., 2019). The total volume of PX-1 borehole is calculated as 85 m^3, with 74 m^3 in the cased portion and 11 m^3 in the lowest (open hole granodiorite) section (Burnside et al., 2019; Banks et al., 2019).

The PX-2 well was drilled and completed as a vertical hole in 2015 to 4348 m depth, with a lowermost 140 m long, 216 mm diameter open hole section (Hofmann et al., 2019).

Five episodes of hydraulic stimulation were applied to wells PX-1 and PX-2 between January 2016 and September 2017 in an attempt to increase reservoir transmissivity and establish an acceptable degree of hydraulic connectivity between the wells (Park et al., 2017). During these five stimulations (Lee et al., 2019), 5663 m^3 water was injected into PX-1 and 7135 m^3 into PX-2 (12,798 m^3 total), while totals of 3968 m^3 and 2989 m^3 (6957 m^3 combined) were recovered as flowback from PX-1 and PX-2, respectively. Thus, a total net unrecovered volume of 5841 m^3 remains in the subsurface (1695 m^3 in PX-1 and 4146 m^3 in PX-2).

Work at the EGS site was terminated following a M_w 5.5 earthquake in the near vicinity on 15th November 2017 (Westaway and Burnside, 2019; Kim et al., 2018; Lee et al., 2019; Grigoli et al., 2018; Zastrow, 2019). An expert panel, appointed by the Republic of Korea government, has reported on this topic and concluded that "*small earthquakes induced by high-pressure injection into the PX-2 well activated the fault that ultimately ruptured in the M_W 5.5 earthquake*" (GSK, 2019; Lee et al., 2019). However, as Fig. 2 indicates, the main shock fault plane and the associated aftershock cluster are more closely concentrated around the bottom of well PX-1. Injection into this well, and chemical effects leading to mineral dissolution within the seismogenic fault, have been considered as an alternative mechanism for causing the large earthquake (Westaway and Burnside, 2019; Westaway et al., 2020).

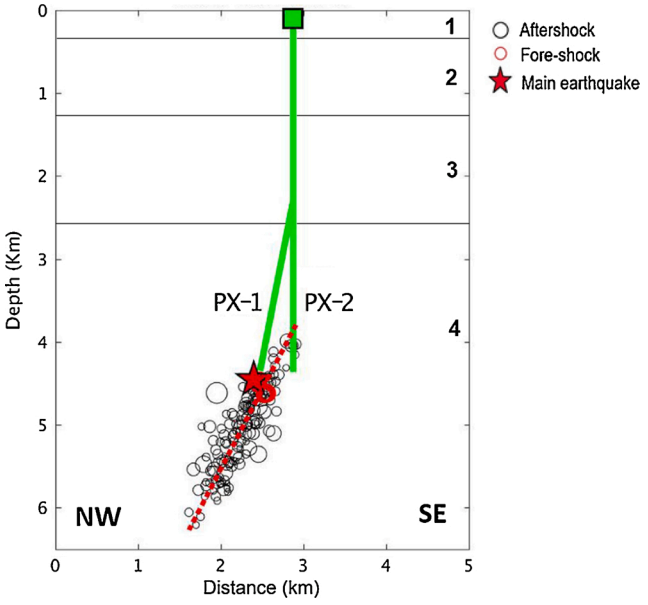

Fig. 2. Schematic section showing the geometric relationship of PX-1 and PX-2 at Pohang; the bottom-hole separation is c. 600 m. Locations of earthquakes at Pohang in November 2017 are also shown, as is the interpreted plane of the Namsong Fault (dashed red line). Modified after (Westaway and Burnside, 2019), which also provides further stratigraphic details. Unit 1 is Middle Miocene marine mudstone (the Yeonil Group, to 206 m depth), underlain by Early Miocene tuff (the Beomgokri Group, to 330 m). Unit 2, dominated by lacustrine mudstone, is latest Cretaceous and Palaeocene (the Yucheon Group, to 1250 m). Unit 3, dominated by subduction-related andesitic lavas and tuffs (the Gyeongsang volcanics, to 2356 m), is Late Cretaceous. Unit 4 is the Permian Pohang Granodiorite. (For interpretation of the references to colour in the Figure, the reader is referred to the web version of this article).

Table 1
Composition (by X-ray diffraction) of air-dried <315 μm fraction of cuttings returned from drilling of well PX-2 at Pohang. Qz = quartz, Pc = plagioclase, Kf = potassium feldspar, Am = amphibole, Ch = chlorite, Mica = illite and muscovite, La = laumontite, Cc = calcite, Gs = gypsum. nd = not detected. This section includes some mafic bodies and fault/fracture gouge mineralisations, including the Namsong fault zone at c. 3800 m. After (GSK, 2019), values rounded to nearest integer. Trace = estimated value <1%.

Depth	Composition (weight %)								
(m)	Qz	Pc	Kf	Am	Ch	Mica	La	Cc	Gs
3535	4	37	17	trace	13	6	16	8	trace
3544	20	48	20	nd	5	2	nd	4	nd
3790	10	43	8	nd	15	10	9	5	nd
3791	6	50	10	nd	19	6	3	6	nd
3792	14	34	17	6	11	12	1	4	nd
3793	8	42	11	10	10	10	5	4	nd
3804	7	45	13	7	11	6	5	6	nd
3807	9	41	10	5	13	11	5	7	nd
3808	5	35	14	6	14	12	8	6	nd
3814	10	35	13	12	11	10	4	5	nd

4. Materials and methods

Hydraulic stimulation at Pohang was typically applied as a series of short-term cyclic injections of surface water, as summarised below and detailed in (Westaway and Burnside, 2019; Kim et al., 2018; Burnside et al., 2019; Park et al., 2017; Lee, 2017; Lee et al., 2019):

- initial stimulation of PX-2; in January – February 2016 (Park et al., 2017)
- initial stimulation of PX-1; in December 2016 - January 2017.
- second stimulation of PX-2; in April 2017.
- second stimulation of PX-1; in August 2017 – reported by (Burnside et al., 2019; Banks et al., 2019; Hofmann et al., 2019).
- third stimulation of PX-2; in September 2017, with wellhead pressures of up to 85 MPa and flow rates of up to 20 L/s (Lee et al., 2019).

This paper specifically considers flowback from the August 2017 stimulation of PX-1.

4.1. August 2017 stimulation of PX-1

The water used for stimulation was primarily sourced from a surface pond for irrigation water – the Namdong No.2 Reservoir - c. 250 m NNE of the borehole site. The site also possesses a shallow groundwater borehole, and it cannot be excluded that some of the water, in the earliest stages of stimulation, may have been derived from this.

For the August 2017 PX-1 stimulation, water was pumped from the pond, with no treatment, to a storage tank, from which it was injected under pressure into the well. For this stimulation, a 180 μm filter had been installed between the initial pond water storage tanks and wellhead storage tanks.

This August 2017 stimulation involved the cyclic injection of c. 1756 m^3 water to PX-1 between 7th and 14th August, at rates of up to 10 L/s and well head pressures of up to c. 23 MPa (Kim et al., 2018; Hofmann et al., 2019; Lee et al., 2019). Following injection, flowback from the well started at 09:34 on 14th August. Flowback water was collected in storage tanks, prior to removal off site by tanker. Flowback rates declined rapidly from over 6 L/s to around 0.6 L/s after c. 140 h flowback (Westaway and Burnside, 2019; Burnside et al., 2019). Between 16th-24th August, works were carried out to remove casing from well PX-1, to permit the installation of a submersible pump at c. 800 m depth. A production test was carried out on PX-1 between 25th August and 1st September 2017, using the submersible pump (Westaway and Burnside, 2019). The total water recovered, via flowback and pumping, following the August 2017 stimulation, is estimated as c. 1771 m^3 (Hofmann et al., 2019), slightly in excess of the volume injected.

4.2. Sampling

A water sampling program was undertaken at the Pohang site. Water from the pond used as a source of injection water (samples SK1 - SK3 from different locations in the pond) was sampled prior to the hydraulic stimulation (3rd August).

On 7th August, the injection water was sampled both before (SK21) and after (SK20) the 180 μm filter in the injection line.

Samples of flowback water from Pohang PX-1 were collected at 2–3 - hly intervals from the commencement of flowback (14th August) until 15th August. Subsequently, sampling frequency was reduced to 2 per day and then to 1 per day (Samples SK22 - SK46). Based on observations of declining flowback rate, sample times were also correlated with cumulative flowback (m^3) at that time (Burnside et al., 2019). No samples were collected in the period 21st - 24th August, due to casing-cutting works. Following 25th August, samples were again collected during production testing (SK47 - SK51). Samples were also collected from well PX-2 (SK52 - SK53, 27th - 28th August).

Finally, a range of bulk samples (SK5 - SK19) acquired and stored by Korean staff from various previous air-lift and bleed-off events from PX-1 and PX-2 in the period Dec. 2016 to 3rd August 2017 were recovered, divided into aliquots, and shipped to the UK for analysis.

The sampling and analysis protocols have previously been described (Burnside et al., 2019), but will be briefly summarized below.

Determinations of pH, temperature, electrical conductivity (EC), and oxidation-reduction potential (ORP) were carried out on site (with the exception of SK47 - SK53) using a Myron Ultrameter II 6PFC instrument (with results corrected to 25 °C), at the points where samples were collected. Following the wellhead and flowback tank determinations, replicate determinations of pH and EC were carried out on sampled water at a site building using a Thermo Scientific Orion Star A329 portable meter.

For logistical reasons, no operations using acid could be carried out in the field (alkalinity titration, acid preservation). Samples SK1 - SK21 (collected 3rd-7th August) were subdivided into the following: (a) 3 × 15 mL filtered (0.45 μm) aliquots in polypropylene screw capped flasks for ion chromatography (IC); (b) 1 × 50 mL unfiltered aliquot in polypropylene screw capped flasks (alkalinity); (c) 3 × 10 mL unfiltered aliquots in glass vials (stable isotope analysis); (d) 3 × unfiltered 10 mL aliquots in glass vials (inductively coupled plasma optical emission spectrometry; ICP-OES).

Samples SK22 - SK53 (collected 14th August onwards) were collected either at the point of entry to the fluid flowback tank or at the wellhead, depending on wellhead operations, and immediately transferred to either 2 × 500 mL or 1 × 1000 mL plastic flasks which were sealed (unfiltered and unacidified) and returned to the University of Glasgow (UoG). On arrival at UoG, these samples were used to prepare filtered and unfiltered sample aliquots as described above

4.3. Analysis

UoG laboratory determinations follow previously documented protocols (Burnside et al., 2016). Anions and cations were measured using Dionex ICS-900 and ICS-1100 Ion Chromatography (IC) equipment. δ^2H and $\delta^{18}O$ stable isotopes were measured using VG Optima and Thermo Scientific Delta V isotope ratio mass spectrometers at the Scottish Universities' Environmental Research Centre (SUERC). ICP-OES (including dissolved silica, major, minor and trace elements) was carried out on laboratory filtered and acidified aliquots by the commercial laboratory CLS, East Kilbride, UK (UKAS accreditation ISO/IEC 17025:2005).

Total alkalinity (corresponding to bicarbonate concentration), was determined at UoG by titration using 0.16 or 1.6 M sulphuric acid, to a pH end-point of c. 4.5 (bromocresol green - methyl red indicator), with Hach Model 16900 digital titrator (Hach Company, Loveland, Colorado).

Sulphur isotopic determinations were made at SUERC on the sulphate fraction of sealed unfiltered aliquots of water samples. Samples were acidified to pH 3–4 using 10 % HCl, then dosed with excess 5% barium chloride solution to precipitate sulphate as barium sulphate (Carmody et al., 1998), which was allowed to settle. This precipitate was recovered from the flask and cleaned repeatedly in de-ionised water, then dried. To analyse sulphur isotopes in this precipitate, SO_2 gas was generated by combustion at 1065 °C with excess Cu_2O and silica (Coleman and Moore, 1978), then measured isotopically using a VG Isotech SIRA II mass spectrometer. The ratio between ^{34}S and ^{32}S was reported as $\delta^{34}S$, as per mille (‰) variations from the Vienna Canyon Diablo Troilite (V-CDT) reference (Beaudoin et al. (1994); Krouse and Coplen (1997)).

$$\delta^{34}S = \left[\frac{\left(^{34}S/^{32}S\right)_{sample} - \left(^{34}S/^{32}S\right)_{reference}}{\left(^{34}S/^{32}S\right)_{reference}}\right] \times 1000 \quad (3)$$

4.4. Quality of data

Degassing, for example of CO_2, and storage can affect analytical quality. For this reason, sensitive parameters such as pH, dissolved oxygen and oxidation-reduction potential were determined in the field. For the last samples (SK47−53) where field determinations were not logistically possible, and where pH was determined in the laboratory, caution should be exercised.

Several of the major ion parameters (SO_4^{2-}, K^+, Na^+, Ca^{2+}, Mg^{2+}) were determined both by IC and ICP-OES. Good correlations were observed between the two data sets, although the correlation for K^+ was somewhat poorer (see Fig. A2 in (Burnside et al., 2019)). A decision was reached to prefer in-house IC data, due to method transparency and generally shorter intervals between sampling and analysis. In (Burnside et al., 2019) and the current paper, the UoG IC data is presented for SO_4^{2-} Na^+, Mg^{2+}, Ca^{2+}, NH_4^+ and all anionic species, while CLS ICP-OES data is cited for K^+, silica and other elements.

Ion balance error was calculated for each of the 57 samples, based on major cations and anions. All samples had an ion balance error of within ±10 % and 42 samples had an ion balance within ±5%, which is typically regarded as sufficiently accurate for groundwaters (Bartram and Ballance, 1996; Misstear et al., 2017).

Five aliquots of sample SK51 were analysed by IC allowing reproducibility to be evaluated. Standard deviations were less than 0.3 % for ions occurring at high concentration (Cl^-, SO_4^{2-}, Na^+), with reproducibility declining for ions occurring at lower concentrations (c. 2.7 % for calcium and 6% for potassium). A standard deviation of 44 % was recorded for Mg^{2+} in sample SK51, where magnesium only occurred at c. 1 mg/L, close to the limit of quantification. Samples SK1 - SK3 of fresh pond water also exhibited good reproducibility by IC with standard deviations for Cl^- SO_4^{2-}, Na^+, Ca^{2+}, Mg^{2+}, K^+ all less than 4%.

Reproducibility of $\delta^{34}S$ of the results was evaluated through repeated analysis of standards NBS-123 (+17.1‰), IAEA-S-3 (-32.3‰), and SUERC's internal standard CP-1 (−4.6‰) and was typically around ±0.3‰ during these analyses.

5. Results

The inorganic chemistry of the flowback water following the August 2017 well stimulation (injection) attempt has already been reported (Burnside et al., 2019; Westaway et al., 2020; Banks et al., 2019); only selected parameters will be discussed in detail in this paper.

5.1. General hydrochemical evolution

The injected surface water was a relatively fresh, oxidising, calcite-undersaturated, circumneutral calcium-sulphate water (Table 2). As flowback progressed, the produced water became increasingly brackish (reaching a 25 °C-corrected EC of c. 3500 µS/cm) and reducing, and began to display a sodium chloride, calcite-saturated composition. Flowback water temperature peaked at 65 °C after 75 h and then declined, due to heat loss during a progressively slower ascent as flowback rate decreased. It has been suggested (Burnside et al., 2019) that the *in-situ* redox condition was iron-, manganese-, and nitrate-reducing, and around the sulphate-reduction threshold. Na^+/Cl^- and Br^-/Cl^- ratios evolved towards values consistent with an ultimately marine origin for salinity. On the other hand, δ^2H and $\delta^{18}O$ tended towards a composition close to the meteoric water line, but somewhat enriched in ^{18}O. This suggests that the produced water originated as meteoric water, but has undergone oxygen isotope exchange with the mineral matrix at elevated temperature (Burnside et al., 2019). In other words, the water and the salinity have differing origins.

Many dissolved solute concentrations, such as chloride (which is typically regarded as conservative), and electrical conductivity exhibit an early rapid increase when plotted against time or (more meaningfully, given that flowback rate decreases with time) cumulative flowback volume. Researchers have fitted two types of idealised curve to the flowback data: (1) a homogeneous mixed tank model (Winkel, 1994), representing the progressive flushing of injected water by in-situ granodiorite fluid, and (2) Sauty's (Sauty, 1980) advective dispersive solute transport model. The former was favoured by (Burnside et al., 2019; Banks et al., 2019) and conceptualises the fracture network and borehole as a combined reservoir; the second was favoured by (Westaway et al., 2020) and regards the fracture network and borehole primarily as a transport conduit. Both approaches produce very similar results that closely fit the data (Fig. 3). The water quality evolves towards that of a putative *in-situ* granodiorite groundwater with a chloride content in excess of 1000 mg/L – although the composition may have been influenced by drilling and the previous well stimulation episode of January 2017. The flowback curves can be normalised, by setting the lowest recorded concentration (usually one of the initial samples) as 0% and the highest recorded value (usually, the final sample) as 100 %. The chloride curve then appears as shown in Fig. 4.

Like chloride, normalised concentrations of many other solutes (e.g. ammonium, arsenic, boron, bromide, strontium and molybdenum (Burnside et al., 2019)) exhibit quasi-conservative behaviour. Fig. 4 shows, for example, that the normalised boron plot approximately coincides with chloride, albeit with a slight deficit at late flowback times.

Table 2
Summary of injection water quality from surface pond and final produced water quality from Pohang PX-1. Nd = not determined. Dissolved oxygen as % saturation. ORP = oxidation-reduction potential. * not measured in field on SK51; cited determinations are the final field determinations for Sample SK46 (20/8/17). ** measured temperature of injection water on 7th August 2017 was 29.6 °C. $ measured in laboratory on SK51.

	Pond water (injection water) Average of SK1 to SK3	Final sample from production testing SK51 dated 1st Sept. 2017
Field determinations		
pH	6.4	7.2 *
Temperature (°C)	31.4 **	47 *
Electrical conductivity (µS/cm)	926	3584 $
ORP (mV)	+169	−183 *
Dissolved oxygen (%)	80	Nd
Total alkalinity by titration		
Total alkalinity (meq/L)	0.51	1.4
IC analysis (mg/L) University of Glasgow		
Sulphate as SO_4^{2-}	336	949
Chloride	57.2	459
Nitrate as NO_3^-	3.5	0.3
Calcium	96.4	181
Magnesium	32.4	1.5
Sodium	51.8	611
ICP-OES analysis (ppm)		
Potassium	10.8	35.6
Silicon as SiO_2	25.3	160
Arsenic	<0.01	0.31
Boron	0.18	12.1
Barium	0.016	0.3
Iron	<0.02	0.81
Manganese	<0.013	0.43
Ion balance		
Sum cations (meq/L)	10.6	36.9
Sum anions (meq/L)	9.2	37.9
Ion balance error	6.6 %	−1.4%
Br^-/Cl^- molar ratio	0.023	0.0019
Isotopic analysis		
δ^2H (‰)	−30.9	−47.9
$\delta^{18}O$ (‰)	−4.5	−6.0
$\delta^{34}S$ (‰)	−17.3	+8.2

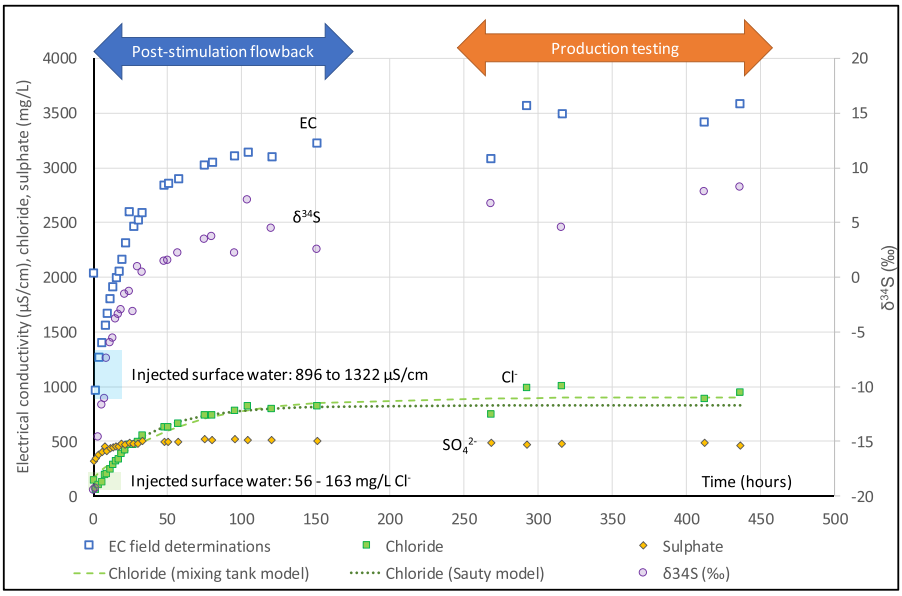

Fig. 3. Electrical conductivity (EC), chloride, sulphate and $\delta^{34}S$ in the flowback water from Pohang PX-1 in August 2017, plotted against time since flowback began. Best fit flushed mixing tank model (Banks et al., 2019) and Sauty advective dispersive model (Westaway et al., 2020) shown for chloride data. The correspondence between time and cumulative flowback is shown in Table 3.

Sodium initially exhibits slight excess concentrations (lying above the chloride curve, Fig. 4), suggesting hydrolysis of silicate minerals by the injected water and release of Na^+ (and K^+ (Burnside et al., 2019)) to the dissolved phase. This effect is even more pronounced in the case of silica: as the cool, silica-poor injected surface water is heated in the granodiorite fracture network, it becomes dramatically undersaturated with respect to quartz, allowing silica to be dissolved rapidly into solution. This temperature-dependence allows dissolved silica to be used as a geothermometer (Burnside et al., 2019; Westaway et al., 2020): assuming quartz to be the controlling silica phase, a reservoir temperature of 165–169 °C is calculated (Fournier, 1977). A chalcedony geothermometer yields a slightly lower figure of 138–142 °C (Arnórsson et al., 1983). These temperatures coincide with independent estimates (Section 3.2). Sulphate also exhibits a significant excess concentration in flowback water (Fig. 4).

5.2. Sulphur isotopes

The ^{34}S isotopic determinations on the selected water samples are presented (along with corresponding sulphate and chloride concentrations) in Table 3, and graphically in Fig. 5. The covariation of $\delta^{34}S$ with sulphate is presented in Fig. 6.

The injected surface water exhibited a relatively high sulphate concentration of 330–360 mg/L and a dissolved sulphate $\delta^{34}S$ of -16.8 to -17.8‰. This highly negative value strongly suggests that the sulphate in the pond water was derived from oxidation of sedimentary sulphide minerals in its catchment. In the initially produced flowback water the value is similarly negative, but thereafter starts to rise, reaching +7‰ after c. 935 m^3 flowback. Subsequently, the value decreased a little, but then rose again to reach +8.2‰ by the end of the production testing (Table 3). The evolutionary trend of the $\delta^{34}S$ lies generally above the

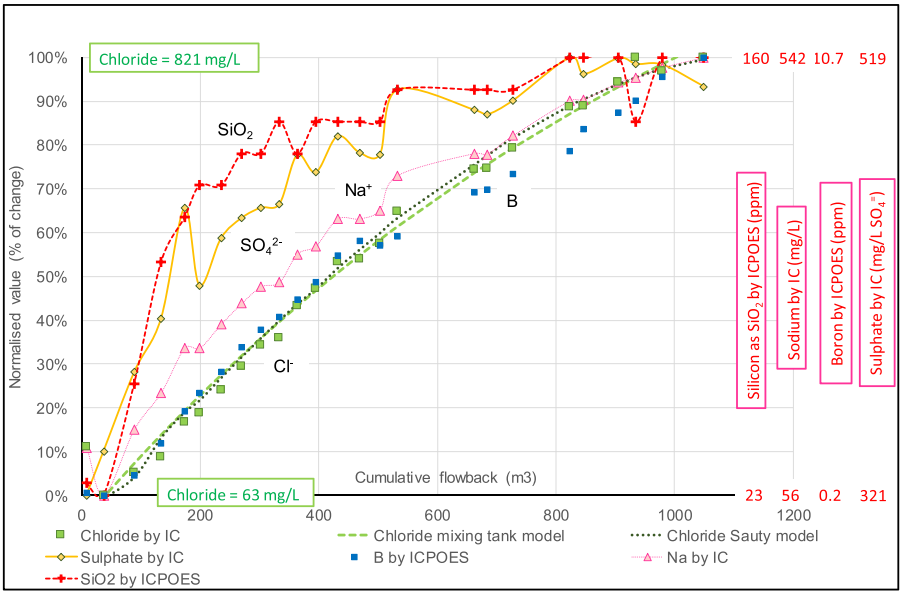

Fig. 4. Silicon (plotted as SiO_2 by ICP-OES), boron (by ICP-OES), sulphate (by IC), sodium (by IC) and chloride concentrations (by IC) in the flowback water from Pohang PX-1 in August 2017, plotted against cumulative flowback. Data are normalised between 0% (lowest concentration) and 100 % (highest concentration).

Table 3
Selected analytical parameters in waters sampled at the Pohang geothermal site (full data set, excluding $\delta^{34}S$, published by (Burnside et al., 2019). Sulphate, chloride and sodium by ion chromatography (IC). t = time and C = cumulative flowback, since flowback commenced.

Sample	Description	Date		Chloride (mg/L)	Sulphate (mg/L)	SO_4^{2-}/Cl^- (molar)	Na^+/Cl^- (molar)	$\delta^{34}S$ (‰)
Standard ocean water (Tostevin et al., 2014; Stanford University, 2019)								
				18,980	2649	0.052	0.86	+20.6
Data from earlier samples								
SK17	PX-1 bleed off	23/12/16		67	405	2.22	1.52	−18.3
SK18	PX-1 bleed off	24/12/16		249	556	0.83	1.91	−1.0
SK19	PX-1 bleed off	20/3/17		963	519	0.20	1.18	+9.8
SK11	PX-1 air lift	2/8/17		996	536	0.20	1.27	+11.6
SK15	PX-2 bleed off	17/1/17		966	478	0.18	0.94	+2.2
SK16	PX-2 bleed off	16/3/17		4686	414	0.03	0.79	+13.1
SK7	PX-2	17/4/17		706	580	0.30	0.88	+6.5
SK8	PX-2 bleed off	03/5/17		2709	326	0.04	0.55	+13.4
Pre-stimulation samples of injection water								
SK1	Pond (injection source)	3/8/17		56	346	2.28	1.39	−16.8
SK2	Pond (injection source)	3/8/17		58	332	2.11	1.38	
SK3	Pond (injection source)	3/8/17		58	330	2.11	1.42	−17.8
SK21	Inj. Water pre-filter	7/8/17		63	355	2.08	1.30	−16.8
SK20	Inj. Water post-filter	7/8/17		163	363	0.82	1.14	−16.8
Flowback water (PX-1)								
		t (hrs)	C (m^3)					
SK22	PX-1 flowback	0.35	8.28	147	321	0.80	1.14	−19.5
SK23	PX-1 flowback	1.60	37.2	63	341	1.99	1.37	−19.3
SK24	PX-1 flowback	3.93	88.9	103	377	1.36	1.94	−14.6
SK25	PX-1 flowback	6.10	134	130	401	1.14	2.02	−11.7
SK26	PX-1 flowback	8.10	174	191	451	0.87	1.78	−11.1
SK27	PX-1 flowback	9.43	199	205	416	0.75	1.65	−7.4
SK28	PX-1 flowback	11.4	235	246	437	0.66	1.54	−6.0
SK29	PX-1 flowback	13.4	270	286	446	0.58	1.45	−5.6
SK30	PX-1 flowback	15.4	303	323	451	0.52	1.37	−3.8
SK31	PX-1 flowback	17.4	334	336	453	0.50	1.34	−3.4
SK32	PX-1 flowback	19.4	364	391	475	0.45	1.28	−3.0
SK33	PX-1 flowback	21.7	395	421	467	0.41	1.22	−1.6
SK34	PX-1 flowback	24.4	432	467	483	0.38	1.20	−1.3
SK35	PX-1 flowback	27.4	469	472	476	0.37	1.19	−3.2
SK36	PX-1 flowback	30.4	503	499	475	0.35	1.15	+0.9
SK37	PX-1 flowback	33.2	532	554	504	0.34	1.14	+0.4
SK38	PX-1 flowback	47.9	663	628	495	0.29	1.07	+1.4
SK39	PX-1 flowback	50.9	684	629	493	0.29	1.07	+1.5
SK40	PX-1 flowback	57.4	728	664	499	0.28	1.06	+2.2
SK41	PX-1 flowback	75.2	823	735	519	0.26	1.04	+3.4
SK42	PX-1 flowback	80.4	847	737	511	0.26	1.04	+3.7
SK43	PX-1 flowback	95.6	906	777	519	0.25	1.02	+2.2
SK44	PX-1 flowback	104.5	935	820	516	0.23	0.98	+7.0
SK45	PX-1 flowback	120.6	980	796	515	0.24	1.03	+4.4
SK46	PX-1 flowback	151.3	1049	821	506	0.23	1.02	+2.5
SK47	PX-1 production test	c. 268		744	491	0.24	1.14	+6.7
SK48	PX-1 production test	c. 292		989	469	0.17	0.95	
SK49	PX-1 production test	c. 316		1003	475	0.17	0.95	+4.5
SK50	PX-1 production test	c. 412		887	489	0.20	1.05	+7.8
SK51	PX-1 production test	c. 436		949	459	0.18	0.99	+8.2
Samples from PX-2 during production testing of PX-1								
SK52	PX-2	c. 316		5658	111	0.007	0.52	+26.9
SK53	PX-2	c. 340		5753	113	0.007	0.52	+24.3

normalised chloride curve (Fig. 5), suggesting that it represents not merely a conservative transition between two end members, but also a component of additional input of ^{34}S-enriched sulphur.

5.3. Well PX-2

In PX-2, the water is much more saline than PX-1 (up to 5750 mg/L chloride, as opposed to up to 1000 mg/L in PX-1, Table 3). Bleed-off water from March and May 2017 had molar SO_4^{2-}/Cl- ratios less than ocean water, and with higher $\delta^{34}S$ (around +13‰) than observed in PX-1. In samples from PX-2 recovered during production testing of PX-1 in August 2017, the molar SO_4^{2-}/Cl- ratio was extremely low (<0.01) and the $\delta^{34}S$ reached +26‰.

6. Discussion

6.1. Source of sulphate in Pohang geothermal reservoir

The fluid chemistry at the end of the flowback – production period in PX-1 is assumed to approach the chemistry of the *in-situ* granodiorite groundwater (albeit possibly modified by previous cyclic injection).

Fig. 7 and Table 3 also show the evolution of the Na^+/Cl^- and SO_4^{2-}/

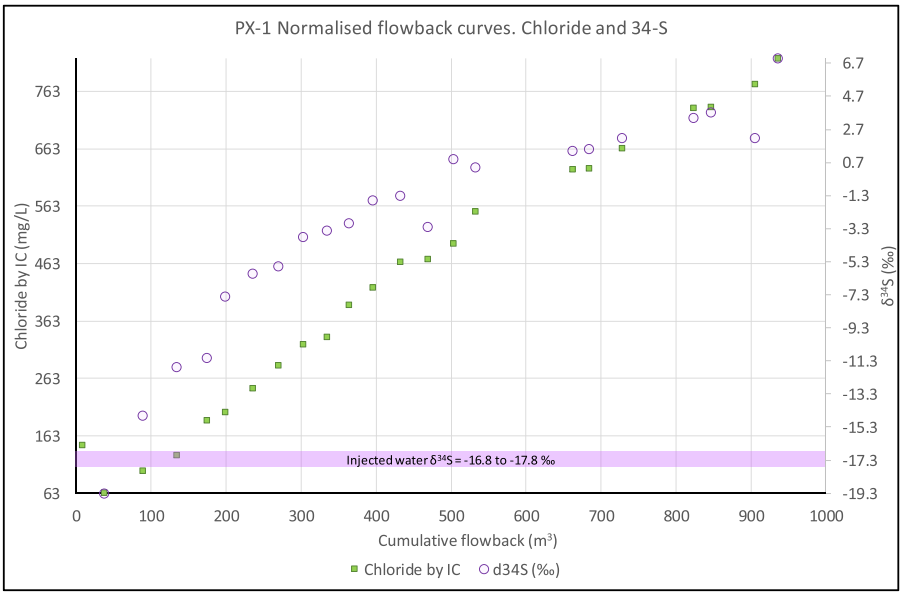

Fig. 5. $\delta^{34}S$ (‰) and chloride concentration (by IC) in the flowback water from Pohang PX-1 in August 2017, plotted against cumulative flowback. Data are normalised between lowest and highest values.

Cl^- molar ratios in the flowback fluid. The Na^+/Cl^- ratio tends towards a marine ratio, suggesting that some components of salinity could be derived from a seawater or halite source. The SO_4^{2-}/Cl^- falls from a ratio of c. 2.1–2.3 (characteristic of the injected water) towards a ratio of around 0.2, significantly higher than the marine value of 0.052 (Stanford University, 2019). This suggests that there is a 'surplus' sulphate content in the *in-situ* granodiorite groundwater, which cannot be explained by marine salts.

The dissolved sulphate $\delta^{34}S$ after extensive flowback is positive and arguably still rising (Fig. 5, Table 3). It thus seems reasonable to assume that the sulphate in the *in-situ* granodiorite formation water has a positive $\delta^{34}S$ of c. + 10‰. Such a value is significantly lower than modern ocean water (+20.6‰ (Tostevin et al., 2014)), or seawater throughout most of the geological past (Bottrell and Newton, 2006). It is also too high to be solely derived solely from oxidation of primary or early stage hydrothermal pyrite of the type reported regionally (Koh et al., 2000; Ishihara et al., 2000) (although late stage hydrothermal pyrite could yield higher $\delta^{34}S$).

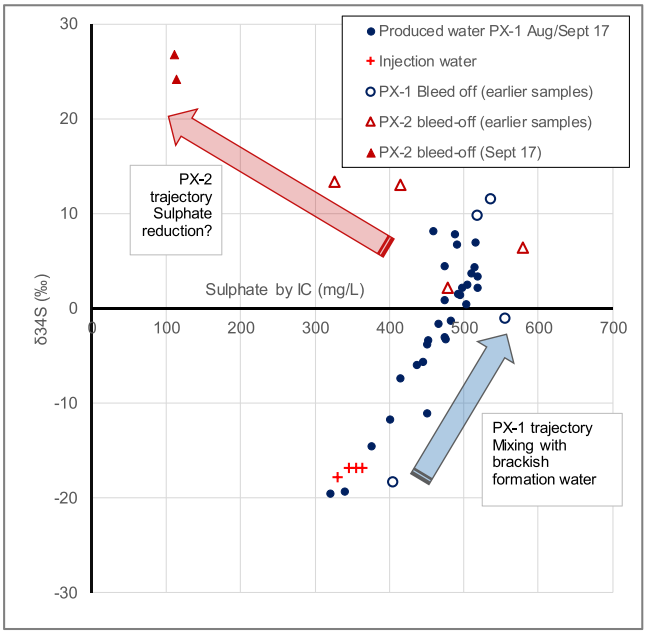

Fig. 6. Sulphate plotted against $\delta^{34}S$ for the water samples in Table 3.

Previous researchers have often found it difficult to explain the origin of sulphate in deep groundwaters with a single hypothesis and have had to invoke multiple sources (Fontes et al., 1989; Banks et al., 2020). With the information available from Pohang, we can merely state that the sulphate in the in situ granodiorite groundwater at Pohang has a likely $\delta^{34}S$ of c. + 10‰ and a concentration, relative to chloride, in excess of that which can be explained by a marine source. It is likely that the sulphate content represents a mixture of:

- ^{34}S-enriched sulphate derived from a marine origin or from dissolution of evaporites in overlying strata (e.g. the Yucheon Group (Chough et al., 2000).
- Sulphate derived from oxidation of sulphides in the granite or overlying strata. Such sulphides could potentially be primary or hydrothermal within the granite (likely $\delta^{34}S$ around 0‰), or secondary sulphides within the granite or overlying sediments (potentially wide range of $\delta^{34}S$ from highly negative to positive).
- Given the known Cretaceous volcanic / hydrothermal activity (Koh et al., 2003, 2000), a disproportionation source of the type described in Eq. 2 is not inconceivable.

When considering the oxidation of sulphides as a source of sulphate in deep groundwater, one should note the paucity of oxidising species in current groundwater (ORP around −160 mV and nitrate < 1 mg/L in late flowback fluid from PX-1). Whilst this implies that in situ pyrite oxidation is currently implausible, it does not preclude episodes of sulphide oxidation in the geological past (e.g. during the Mesozoic, when the granodiorite was exposed to subaerial conditions).

6.2. *Well PX-2*

Before progressing to consider the source of excess sulphate in the flowback fluid from PX-1, it is instructive to examine the chemistry and $\delta^{34}S$ of water sourced from PX-2. The granodiorite water chemistry is very different in the hydrogeological niche around PX-1 from that in PX-2 (Section 5.3). This suggests, at the very least, stratification or compartmentalisation of the aquifer hydrogeochemistry. It has been suggested that the Namsong fault itself represents a low permeability

barrier between the reservoirs accessed by the two boreholes (Westaway et al., 2020). The sulphate deficit relative to marine water, and the strong inverse relationship in PX-2 between $\delta^{34}S$ and sulphate concentration (Fig. 6), are suggestive of sulphate reduction, with accompanying isotopic fractionation. This could be thermochemical sulphate reduction (TSR) at reservoir depth, although fractionations accompanying TSR are modest (typically ≤20‰ (Machel, 2001)). It could also represent bacterial sulphate reduction (BSR) within the well bore itself at a depth where the temperature is low enough to permit it. We speculate that BSR could be favoured in a relatively "stagnant" well bore (PX-2 had not been stimulated since April 2017), where injection of untreated surface water could have provided nutrients and inorganic carbon required by the microbiota, and could even have "seeded" the borehole with microorganisms (Lawson et al., 2016).

6.3. Source of excess sulphate in flowback water

An excess of sulphate in the August 2017 flowback water from PX-1, relative to the normalised conservative chloride curve (Fig. 4) cannot be explained by simple dispersion or mixing processes. We propose that there are two possible sources in the granite for this "pulse" of excess sulphate: (1) dissolution of sulphate minerals, most likely along fracture surfaces, or (2) oxidation of primary/hydrothermal or secondary sulphides. The sulphur isotope trajectory during flowback suggests that the source of the excess sulphate had a $\delta^{34}S$ significantly >0‰ (Fig. 5).

Primary and hydrothermal pyrite often has a $\delta^{34}S$ around or slightly above 0‰. Hydrothermal sulphide infills (pyrite; FeS_2) are observed in fractures within outcrops of granite that form part of the same magmatic suite as the Pohang granodiorite, with a typical $\delta^{34}S$ around 0‰ (-10 to +10‰), but occasionally somewhat higher (Koh et al., 2000, 2003). During the granodiorite's Mesozoic subaerial exposure, it is conceivable that secondary sulphides could have formed from chemical or microbiologically mediated processes, the latter involving sulphate-reducing bacteria. Such BSR is widely observed elsewhere to result in sulphide isotopic compositions ranging from highly ^{34}S-depleted to highly enriched (Drake et al., 2013). More recent isotopic exchange at high depth and temperature (Seal, 2006) could also have tended to equilibrate the sulphide $\delta^{34}S$ with the granodiorite reservoir fluid (c. + 10‰).

Secondary sulphates typically reflect closely the dissolved sulphate sulphur isotope composition of the reservoir fluid from which they were precipitated (Drake and Tullborg, 2009). Given the high concentrations of calcium and sulphate in the reservoir fluid, the main candidate mineral at the reservoir temperature is likely to be anhydrite ($CaSO_4$).

Saturation indices (SI) have been calculated (Burnside et al., 2019) for various mineral phases, relative to the chemistry of the flowback fluid under wellhead temperature and pressure conditions, but also at putative reservoir temperature and pressure conditions (Fig. 8). While the flowback water was undersaturated with respect to gypsum and anhydrite at wellhead conditions, it was calculated to be oversaturated with respect to anhydrite under reservoir temperature and pressure conditions. We thus hypothesise that, in the granodiorite reservoir, anhydrite has been able to precipitate in fracture surfaces as an alteration mineral, with approximately the same $\delta^{34}S$ as the *in-situ* granodiorite groundwater's dissolved sulphate (c. + 10‰).

From Fig. 4, the normalised sulphate curve lies up to c. 50 mg/L above the conservative chloride trajectory. We can thus evaluate whether anhydrite dissolution or pyrite oxidation can deliver such a concentration of excess sulphate to the flowback water. The speciation and saturation indices of the injection water (SK21) can be simulated in the model PHREEQC (Parkhurst and Appelo, 2013) under both surface conditions (1 atmosphere, 29.6 °C) and reservoir conditions (up to 160 °C, estimated 416 atm. or 42.2 MPa). Table 4 indicates that the injection water, though highly undersaturated at surface temperatures, is saturated with respect to anhydrite at 160 °C; in fact, it becomes saturated >155 °C. This implies that, during the warming process, there is a significant temperature 'window' when it is significantly undersaturated and could dissolve anhydrite from the granodiorite (if present). At 70 °C, for example, the anhydrite saturation index of the injection water is -1.11. If allowed to equilibrate with anhydrite and calcite at 70 °C, 1 L of injection water has the capacity to dissolve 15.15 mmol anhydrite, releasing 1456 mg sulphate to solution and a similar molar quantity of calcium. Even allowing for reprecipitation of some of the anhydrite at higher temperatures, this seems to demonstrate that anhydrite dissolution is a feasible mechanism for generating the observed sulphate excess.

In the case of pyrite:

$$2FeS_2 + 7O_2 + 2H_2O = 2Fe^{2+} + 4SO_4^{2-} + 4H^+ \quad (4)$$

7 mmol oxygen (224 mg) can oxidise 2 mmol pyrite (240 mg) to release 2 mmol ferrous iron (112 mg) and 4 mmol sulphate (384 mg). The solubility of atmospheric oxygen in water at 25 °C is 8.2 mg/L (0.26 mmol/L; (Xing et al., 2014)). Thus, if the injection water was fully

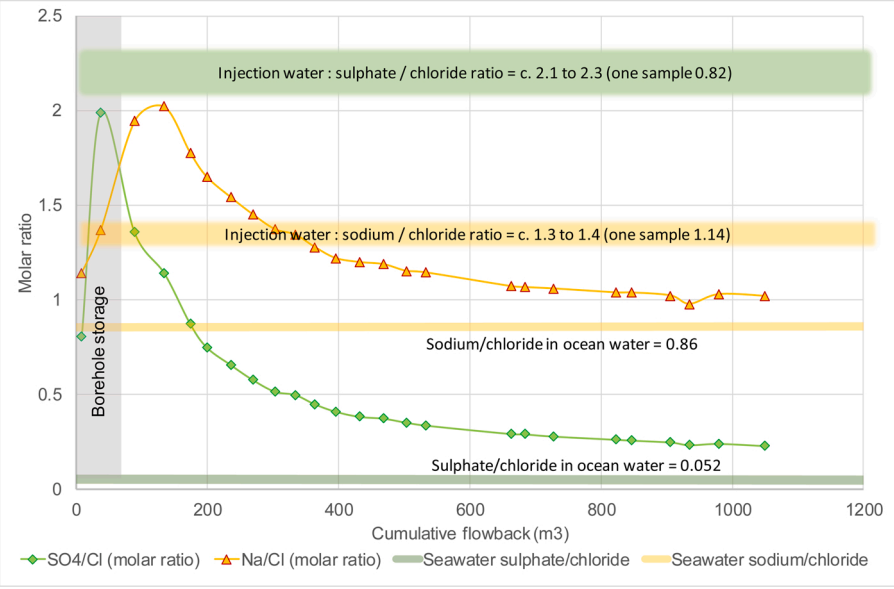

Fig. 7. Molar ratios of sulphate/chloride and sodium/chloride in flowback water from Pohang borehole PX-1 in August 2017, versus cumulative flowback. The grey shading on the left indicates that the first two samples did not enter the granodiorite reservoir and represent borehole storage of injected water.

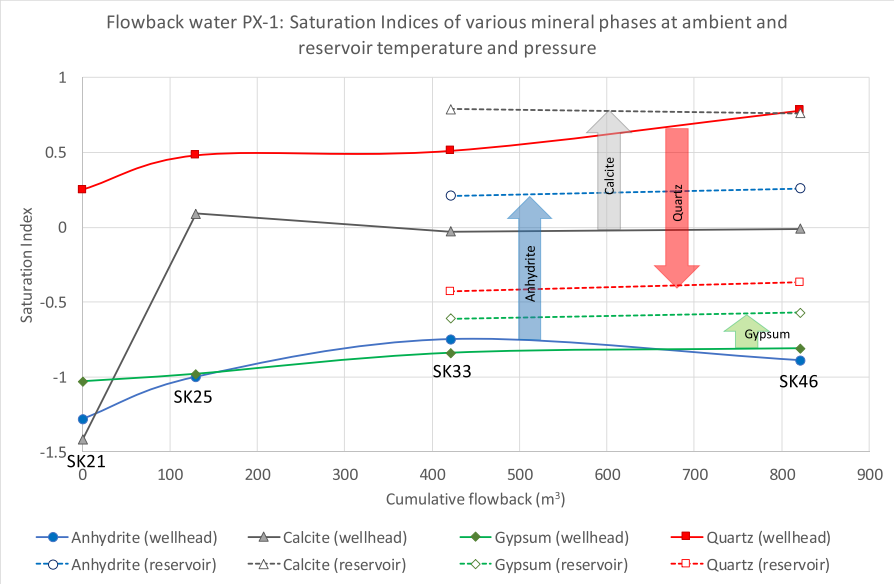

Fig. 8. Calculated saturation indices, using PHREEQC (Parkhurst and Appelo, 2013), for PX-1 flowback water under wellhead/sample temperature and atmospheric pressure and at putative reservoir temperature and pressure (160 °C and 42.2 MPa, 416 atm.) after data in (Burnside et al., 2019). Sample SK21 represents injection water. Arrows show shift in SI due to reservoir temperature and pressure.

saturated with oxygen, it would only be capable of oxidising 0.07 mmol/L pyrite and releasing 4 mg/L iron and 14 mg/L sulphate. The stoichiometry for other sulphides is even less favourable: for example, 8 mmol oxygen oxidise 4 mmol sphalerite (ZnS) to release 4 mmol sulphate.

The process can also be simulated in the hydrochemical model PHREEQC (Parkhurst and Appelo, 2013). 8.2 mg/L oxygen is added to the injection water (to simulate saturation). This is 'generous' as the injection water had a measured temperature of 29.6 °C rather than 25 °C, and the measured dissolved oxygen saturation varied between 63 and 88 %. The water is equilibrated in the model with pyrite and calcite at reservoir pressure and temperature, allowing anhydrite to precipitate if oversaturated. The modelling predicts the dissolution of 0.0097 mmol pyrite per litre at 70 °C and 0.0098 mmol at 160 °C, releasing only 2 mg/L sulphate at 70 °C (and this sulphate is reprecipitated as anhydrite at 160 °C) and 0.54 mg/L iron. The amount of pyrite oxidised is lower than predicted by Eq. (4) because the injection water also contains c. 7 mg/L ammonium, which consumes much of the available oxygen.

Comparable modelling of sphalerite oxidation produces similarly low sulphate concentrations. We thus conclude that sulphide oxidation is stoichiometrically inadequate to account for the observed sulphate excess in the flowback water.

PHREEQC has also been used to verify whether barite dissolution could contribute significant sulphate. Simulations indicate that the injection water could dissolve only 0.4 µmol barite per litre under downhole conditions, due to its low solubility.

Moreover, PHREEQC was used to demonstrate that, under prevailing circumneutral pH conditions, the hydroxysulphate alunite, which is occasionally observed as an alteration mineral resulting from late Cretaceous magmatic hydrothermal activity regionally (Koh et al., 2000; Yoon and Jung, 2008), is highly undersaturated under reservoir conditions. It is thus not regarded as a likely component of the deep

Table 4
Results of PHREEQC (Parkhurst and Appelo, 2013) modelling of the injection water sample SK21, under ambient (29.6 °C and 1 atmosphere) and reservoir (70 to 160 °C and 416 atm.) conditions, allowing equilibration with various minerals species. n/a = not applicable, < = iron lower than detection limit in injection water.

Initial conditions						
Temperature (°C)	29.6	70	160	70	70	160
Pressure (atm)	Atmospheric	416	416	416	416	416
Dissolved oxygen (mg/L)	n/a	n/a	n/a	n/a	8.2	8.2
PHREEQC Conditions	Speciation only			Equilibrate with anhydrite and calcite	Equilibrate with pyrite and calcite, allow anhydrite to precipitate	
Resulting Saturation Indices						
Anhydrite	−1.28	−1.11	+0.05	0	−1.06	0
Barite	−0.21	−0.8	−0.79	−0.59	−0.82	−0.83
Calcite	−1.42	−1.08	−0.23	0	0	0
Gypsum	−1.03	−1.21	−0.77	−0.09	−1.15	−0.82
Resulting concentrations						
Ca (mg/L)	107.5	107.5	107.5	725	127	102
SO_4^{2-} (mg/L)	355	355	355	1810	357	328
Fe (mg/L)	<	<	<	<	0.54	0.54
Mineral dissolution (positive) or precipitation (negative)						
Pyrite (mmol/L)	n/a	n/a	n/a	n/a	+0.0097	+0.0098
Calcite (mmol/L)	n/a	n/a	n/a	+0.259	+0.486	+0.156
Anhydrite (mmol/L)	n/a	n/a	n/a	+15.15	0	−0.303
Comment					Goethite oversaturated	

granodiorite reservoir and not tenable as a source mineral for excess sulphate.

Finally, one can speculate that, if anhydrite dissolution were the source of excess sulphate in the flowback, there might be some correlation with calcium. If pyrite were the source of the sulphate, one might expect to see either a correlation with dissolved iron, a negative correlation with pH or a correlation with base cations released by proton hydrolysis. Fig. 9 plots all of these potential correlations on a single diagram.

The sulphate data exhibit a significant excess in the flowback water, which is highest between 100 and 700 m^3 cumulative flowback. This is not clearly reflected in the calcium data, which exhibits an initial decline then closely follows the chloride trajectory, although does tentatively show a modest excess in the region 300 - 600 m^3. There is some indication of correlation in the detail of the IC data for Ca and SO_4^{2-} in Fig. 9; we suspect this may be partially due to salinity interference and method-specific (IC) factors. There is, however, little clear correlation in the overall trends between Ca and SO_4^{2-} in the flowback water, although one might expect calcium solubility to also be controlled by calcite dissolution and precipitation, interactions with silicates and ion exchange, rather than solely by anhydrite dissolution.

pH exhibits a decline from around 50–400 m^3, but iron concentrations exhibit a "deficit" relative to the conservative chloride trajectory, suggesting that iron solubility is supressed by the injection water (indeed, PHREEQC modelling suggests oversaturation with respect to goethite, suggesting iron may be immobilised in ferric form by any residual oxygen in the injected surface water). It is only in the late flowback samples that iron concentrations increase dramatically, reaching over 3 mg/L (higher than predicted by pyrite oxidation – Eq. 4), suggesting an alternative mechanism for iron mobilisation in the in situ granodiorite groundwater; for example, reductive dissolution of iron minerals (Burnside et al., 2019).

7. Conclusions

Boreholes PX-1 and PX-2 at Pohang appear to have intersected different groundwater niches within the deep granodiorite reservoir. The granodiorite groundwater at PX-1 was brackish (>1000 mg/L chloride) and relatively sulphate-rich (>500 mg/L) with a sulphate/chloride ratio exceeding seawater and a sulphate $\delta^{34}S$ around +10‰. The water from PX-2 was considerably more saline (up to 5700 mg/L chloride) but showed indications of either thermochemical (within reservoir) or microbial (within borehole) sulphate reduction processes affecting dissolved sulphate concentrations and isotopic compositions.

While some components of the salinity in PX-1 may indicate a marine source, the sulphate/chloride ratio is too high to ascribe a marine origin to most of the sulphate. The reservoir sulphate concentration and its $\delta^{34}S$ will depend on the dynamic equilibrium between various possible sources (marine water, sulphate minerals in the overlying sediments, sulphide minerals in the granodiorite or overlying sediments) and sinks (sulphur removal via sulphate reduction or sulphate precipitation).

Water injected to borehole PX-1 at Pohang in August 2017 contained

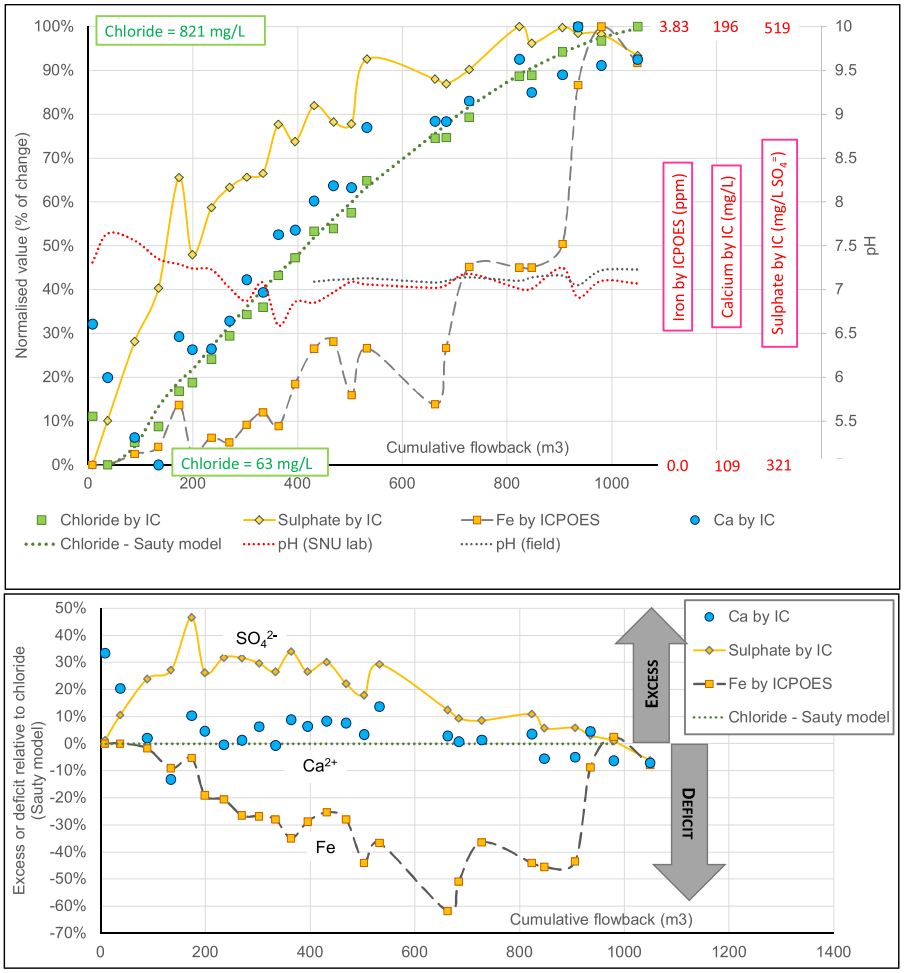

Fig. 9. pH, sulphate, chloride, iron and calcium concentrations the flowback water from Pohang PX-1 in August 2017, plotted against cumulative flowback. In the upper diagram, data are normalised between 0% (lowest concentration) and 100 % (highest concentration). In the lower diagram, excesses or deficits relative to the conservative chloride trajectory (Sauty model) are presented. pH is presented both as field data and as laboratory determinations by Seoul National University (SNU).

c. 330–360 mg/L sulphate, with a highly negative $\delta^{34}S$. As post-stimulation flowback progressed, the water became more saline, the sulphate and chloride contents increased and the sulphate $\delta^{34}S$ became increasingly positive. Compared with conservative advective-dispersive and mixing models, the injection of water released surplus sulphate to the flowback, via water-rock interaction, which had a relatively high $\delta^{34}S$.

In PX-1, the reservoir fluid is saturated with respect to anhydrite at downhole temperatures and pressures. Anhydrite is likely to exist as an alteration product along fracture surfaces, with a relatively ^{34}S-enriched sulphate isotopic composition corresponding to the *in-situ* fluid's dissolved sulphate (i.e. around +10‰). The granodiorite is also likely to contain pyrite mineralisation on fracture surfaces, of unknown isotopic composition, though determinations of hydrothermal pyrite at surface outcrops have tended to yield values in the range -10 to +10‰ (Koh et al., 2000). Injection of cool, anhydrite-undersaturated surface water, with a content of dissolved oxygen, could have dissolved either anhydrite or pyrite from granodiorite fracture surfaces, appearing in the flowback as an excess of sulphate.

PHREEQC (Parkhurst and Appelo, 2013) modelling indicates that at 70 °C the injection water has the capacity to dissolve up to 15.15 mmol anhydrite per litre of water, releasing up to 1450 mg/L sulphate. Stoichiometry suggests that the same water could have oxidised up to 0.07 mmol pyrite per litre, releasing 14 mg/L sulphate. However, PHREEQC modelling suggests that much of the available oxygen would have been consumed oxidising ammonium, resulting the in the oxidation of <0.01 mmol pyrite per litre, and the release of as little as 2 mg/L sulphate. Given that the flowback water contained excess sulphate concentrations of up to 50 mg/L, anhydrite dissolution is the preferred hypothesis.

Previous work (Westaway and Burnside, 2019; Burnside et al., 2019; Westaway et al., 2020) demonstrates that the injection of cool silica-poor surface water at depth into a hot granodiorite reservoir was able to solubilise significant quantities of quartz from fracture surfaces. This work has demonstrated that injection of surface water (which may be undersaturated with respect to several other minerals in the reservoir assemblage) has also been able to mobilise sulphate from the reservoir, most likely by the dissolution of secondary anhydrite from fracture surfaces. Anhydrite dissolution by injected water could increase the anhydrite, gypsum or barite scaling potential of produced geothermal water in an EGS system. Moreover, mineral dissolution within a seismogenic fault by injected surface water can be considered as a supplementary mechanism facilitating seismic slip (Westaway and Burnside, 2019; Westaway et al., 2020).

Data availability

The full hydrogeochemical data set from the Pohang hydraulic stimulation has been published as supplementary material (Appendix B) to (Burnside et al., 2019), and is available at https://doi.org/10.1016/j.apgeochem.2019.104445. The sulphur isotope data additional to this published data set are contained in Table 3 of this paper.

Funding

This work was funded by the European Commission Horizon 2020 LCE 'DESTRESS' project (grant number EC-691728). AJB was funded by SUERC and the NERC Facilities, with isotopic analyses carried out at the ICSF in SUERC (NERC Facility contract number F14/G6/11/01). NMB was supported by a University of Glasgow Lord Kelvin Adam Smith Research Fellowship.

CRediT authorship contribution statement

David Banks: Conceptualization, Formal analysis, Writing - original draft. **Adrian J. Boyce:** Resources, Writing - review & editing. **Rob Westaway:** Conceptualization, Investigation, Formal analysis, Writing - review & editing. **Neil M. Burnside:** Conceptualization, Resources, Investigation, Writing - review & editing, Project administration.

Declaration of Competing Interest

The authors declare that they have no known competing financial interests or personal relationships that could have appeared to influence the work reported in this paper.

Acknowledgements

We thank: NexGeo for access to the Pohang site for sampling; Anne McGarrity and Alison McDonald for analyses; Eunhyea Chung and Ki-Bok Min, and their respective teams, of Seoul National University for collecting samples and providing additional data; and many DESTRESS co-workers for helpful discussions. Günter Zimmermann and Hannes Hofmann of the German GeoForschungsZentrum (GFZ) collected data on flowback rate. We especially thank Paul Younger (deceased 21 April 2018), who led UoG involvement in DESTRESS and helped to secure the funding for this work.

References

Aquilina, L., Armandine-Les Landesa, A., Ayraud-Vergnauda, V., Labasquea, T., Roques, C., Davy, P., Pauwels, H., Petelet-Giraud, E., 2013. Evidence for a saline component at shallow depth in the crystalline Armorican basement (W France). Procedia Earth Planet. Sci. 7, 19–22. https://doi.org/10.1016/j.proeps.2013.03.157.

Arnórsson, S., Gunnlaugsson, E., Svavarsson, H., 1983. The chemistry of geothermal waters in Iceland. III. Chemical geothermometry in geothermal investigations. Geochim. Cosmochim. Acta 47 (3), 567–577. https://doi.org/10.1016/0016-7037(83)90278-8.

Balashov, V.N., Engelder, T., Gu, X., Fantle, M.S., Brantley, S.L., 2015. A model describing flowback chemistry changes with time after Marcellus Shale hydraulic fracturing. AAPG Bull. 99 (1), 143–154. https://doi.org/10.1306/06041413119.

Banks, D., Burnside, N., Westaway, R., Zimmermann, G., Hofmann, H., 2019. Exponential trends in flowback chemistry from a hydraulically stimulated deep geothermal borehole in granite; Pohang, South Korea. In: Proc. 16th International Symposium on Water-Rock Interaction and 13th International Symposium on Applied Isotope Geochemistry (1st IAGC International Conference) July 21-26, 2019. Tomsk, Russia.

Banks, D., Boyce, A.J., Burnside, N., Janson, E., Roqueñi Gutierrez, N., 2020. On the common occurrence of sulphate with elevated δ34S in European mine waters: sulphides, evaporites or seawater? Int. J. Coal Geology 232. https://doi.org/10.1016/j.coal.2020.103619 article 103619.

Bartram, J., Ballance, R., 1996. Water quality monitoring: a practical guide to the design and implementation of freshwater quality studies and monitoring programs. E & FN Spon on behalf of United Nations Environment Programme and the World Health Organization, London.

Bayon, F.E.B., Ferrer, H., 2005. Sulphur isotope ratios in Philippine geothermal system." In Use of isotope techniques totrace the origin of acidic fluids ingeothermal systems. IAEA Publication IAEA-TECDOC-1448. International Atomic Energy Agency (IAEA), Vienna, Austria, pp. 111–132.

Beaudoin, G., Taylor, B.E., Rumble, D., Thiemens, M., 1994. Variations in the sulfur isotope composition of troilite from the Cañon Diablo iron meteorite. Geochim. Cosmochim. Acta 58 (19), 4253–4255. https://doi.org/10.1016/0016-7037(94)90277-1.

Böttcher, M.E., 2011. In: Reitner, J., Dordrecht, Thiel V. (Eds.), "Sulfur isotopes." In *Encyclopedia of Geobiology (Encyclopedia of Earth Sciences Series)*. Springer, Dordrecht, Netherlands. https://doi.org/10.1007/978-1-4020-9212-1.

Bottomley, D.J., Gregoire, D.G., Raven, K.G., 1994. Saline groundwaters and brines in the Canadian Shield: geochemical and isotopic evidence. Geochim. Cosmochim. Acta 58 (5), 1483–1498. https://doi.org/10.1016/0016-7037(94)90551-7.

Bottrell, S.H., Newton, R.J., 2006. Reconstruction of changes in global sulfur cycling from marine sulfate isotopes. Earth Sci. Rev. 75, 59–83. https://doi.org/10.1016/j.earscirev.2005.10.004.

Bottrell, S.H., Moncaster, S.J., Tellam, J.H., Lloyd, J.W., Fisher, Q.J., Newton, R.J., 2000. Controls on bacterial sulphate reduction in a dual porosity aquifer system: the Lincolnshire Limestone aquifer, England. Chem. Geol. 169 (3), 461–470. https://doi.org/10.1016/S0009-2541(00)00222-9.

Brady, P., Lopez, C., Sassani, D., 2019. Granite hydrolysis to form deep brines. Energies 12. https://doi.org/10.3390/en12112180. Article 2180.

Brehme, M., Nowak, K., Banks, D., Petrauskas, S., Valickas, R., Bauer, K., Burnside, N., Boyce, A., 2019. A review of the hydrochemistry of a deep sedimentary aquifer and its consequences for geothermal operation: Klaipeda, Lithuania. Geofluids 2019. https://doi.org/10.1155/2019/4363592. Article 4363592.

Bucher, K., Stober, I., 2010. Fluids in the upper continental crust. Geofluids 10 (1-2), 241–253. https://doi.org/10.1111/j.1468-8123.2010.00279.x.

Burnside, N.M., Banks, D., Boyce, A.J., 2016. Sustainability of thermal energy production at the flooded mine workings of the former Caphouse Colliery, Yorkshire, United Kingdom. Int. J. Coal Geology 164, 85–91. https://doi.org/10.1016/j.coal.2016.03.006.

Burnside, N.M., Westaway, R., Banks, D., Zimmermann, G., Hofmann, H., Boyce, A.J., 2019. Rapid water-rock interactions evidenced by hydrochemical evolution of flowback fluid during hydraulic stimulation of a deep geothermal borehole in granodiorite: Pohang, Korea. Appl. Geochem. 111. https://doi.org/10.1016/j.apgeochem.2019.104445. Article 104445.

Carmody, R.W., Plummer, L.N., Busenberg, E., Coplen, T.B., 1998. Methods for Collection of Dissolved Sulfate and Sulfide and Analysis of Their Sulfur Isotopic Composition. USGS Open-file Report 97-234. United States Geological Survey, Reston, Virginia, USA. https://doi.org/10.3133/ofr97234. Accessed 9 21, 2019.

Choi, J., Shin, D., Im, H., 2018. Regional variations of sulfur isotope compositions for metallic deposits in the Taebaeksan mineralized district, South Korea. Geosci. J. 22 (1), 79–89. https://doi.org/10.1007/s12303-017-0057-x.

Chough, S.K., Kwon, S.T., Ree, J.H., Choi, D.K., 2000. Tectonic and sedimentary evolution of the Korean peninsula: a review and new view. Earth-Sci. Rev. 52 (1-3), 175–235. https://doi.org/10.1016/S0012-8252(00)00029-5.

Coleman, M.L., Moore, M.P., 1978. Direct reduction of sulfates to sulfur dioxide for isotopic analysis. Anal. Chem. 50 (11), 199–260. https://doi.org/10.1021/ac50033a056.

Cross, M.M., Bottrell, S.H., 2000. Reconciling experimentally observed sulphur isotope fractionation during thermochemical sulphate reduction (TSR) with field data: a "*steady-state*" model of isotopic behaviour. J. Conf. Abstracts (Cambridge Publications) 5 (2), 325.

Ding, K., 2015. Thermal sulfate reduction by ammonium ion (NH_4^+): implications for inorganic origin of H_2S and N_2 in sedimentary basins. Carbonates Evaporites 30, 273–279. https://doi.org/10.1007/s13146-014-0208-3.

Drake, H., Tullborg, E.L., 2009. Paleohydrogeological events recorded by stable isotopes, fluid inclusions and trace elements in fracture minerals in crystalline rock, Simpevarp area, SE Sweden. Appl. Geochem. 24, 715–732. https://doi.org/10.1016/j.apgeochem.2008.12.026.

Drake, H., Tullborg, E.L., Hogmalm, K.J., Aström, M.E., 2012. Trace metal distribution and isotope variations in low-temperature calcite and groundwater in granitoid fractures down to 1 km depth. Geochim. Cosmochim. Acta 84, 217–238. https://doi.org/10.1016/j.gca.2012.01.039.

Drake, H., Åström, M.E., Tullborg, E.L., Whitehouse, M., Fallick, A.E., 2013. Variability of sulphur isotope ratios in pyrite and dissolved sulphate in granitoid fractures down to 1 km depth – evidence for widespread activity of sulphur reducing bacteria. Geochim. Cosmochim. Acta 102, 143–161. https://doi.org/10.1016/j.gca.2012.10.036.

Fike, D.A., Bradley, A.S., Rose, C.V., 2015. Rethinking the ancient sulphur cycle. Annu. Rev. Earth Planet. Sci. 43, 593–622. https://doi.org/10.1146/annurev-earth-060313-054802.

Fontes, J.C., Fritz, P., Louvat, D., Michelot, J.L., 1989. Aqueous sulphates from the Stripa groundwater system. Geochim. Cosmochim. Acta 53 (8), 1783–1789. https://doi.org/10.1016/0016-7037(89)90299-8.

Fournier, R.O., 1977. Chemical geothermometers and mixing models for geothermal systems. Geothermics 5, 41–50. https://doi.org/10.1016/0375-6505(77)90007-4.

Grigoli, F., Cesca, S., Rinaldi, A.P., Manconi, A., López-Comino, J.A., Clinton, J.F., Westaway, R., Cauzzi, C., Dahm, T., Wiemer, S., 2018. The November 2017 Mw 5.5 Pohang earthquake: a possible case of induced seismicity in South Korea. Science 360 (6392), 1003–1006. https://doi.org/10.1126/science.aat2010.

GSK, 2019. Final Report of the Korean Government Commission on Relations Between the 2017 Pohang Earthquake and EGS Project (in Korean). Geological Society of Korea, Seoul, Korea. https://doi.org/10.22719/KETEP-2019043001, 427.

Gudmundsson, B.T., Arnórsson, S., 2002. Geochemical monitoring of the Krafla and Námafjall geothermal areas, N-Iceland. Geothermics 31 (2), 195–243. https://doi.org/10.1016/S0375-6505(01)00022-0.

Haluszczak, L.O., Rose, A.W., Kump, L.R., 2013. Geochemical evaluation of flowback brine from Marcellus gas wells in Pennsylvania, USA. Appl. Geochem. 28, 55–61. https://doi.org/10.1016/j.apgeochem.2012.10.002.

Hofmann, H., Zimmermann, G., Farkas, M., Huenges, E., Zang, A., Leonhardt, M., Kwiatek, G., et al., 2019. First field application of cyclic soft stimulation at the Pohang Enhanced Geothermal System site in Korea. Geophys. J. Int. 217 (2), 926–949. https://doi.org/10.1093/gji/ggz058.

Ishihara, S., Jin, M.S., Sakai, A., 2000. Source diversity of ore sulfur from Mesozoic-Cenozoic mineral meposits in the Korean Peninsula Region. Resour. Geol. 50 (4), 203–212. https://doi.org/10.1111/j.1751-3928.2000.tb00070.x.

Jia, L., Cia, C., Yang, H., Li, H., Wang, T., Zhang, B., Jiang, L., Tao, X., 2015. Thermochemical and bacterial sulfate reduction in the Cambrian and Lower Ordovician carbonates in the Tazhong Area, Tarim Basin, NW China: evidence from fluid inclusions, C, S, and Sr isotopic data. Geofluids 15, 421–437. https://doi.org/10.1111/gfl.12105.

Jo, J., Shin, D., 2015. Sulfur isotope variations of metallic ore deposits in the Gyeongsang Basin, South Korea. Resour. Geol. 65 (3), 296–310. https://doi.org/10.1111/rge.12072.

Kim, H.C., Lee, Y., 2007. Heat flow in the Republic of Korea. J. Geophys. Res. 112 https://doi.org/10.1029/2006JB004266. Article B05413.

Kim, K.-H., Ree, J.-H., Kim, Y.-H., Kim, S., Kang, S.-Y., Seo, W., 2018. Assessing whether the Mw 5.4 Pohang earthquake in South Korea was an induced event. Sci. 360 (6392), 1007–1009. https://doi.org/10.1126/science.aat6081.

Kiyosu, Y., Krouse, H.R., 1990. The role of organic acid in the abiogenic reduction of sulfate and the sulfur isotope effect. Geochem. J. 24, 21–27.

Koh, S.M., Takagi, T., Kim, M.Y., Naito, K., Hong, S.S., Sudo, S., 2000. Geological and geochemical characteristics of the hydrothermal clay alteration in South Korea. Resour. Geol. 50 (4), 229–242. https://doi.org/10.1111/j.1751-3928.2000.tb00072.x.

Koh, S.M., Ryoo, C.R., Song, M.S., 2003. Mineralization characteristics and structural controls of hydrothermal deposits in the Gyeongsang Basin, South Korea. Resour. Geol. 53 (3), 175–192. https://doi.org/10.1111/j.1751-3928.2003.tb00168.x.

Kohut, M., Recio, C., 2002. Sulphur isotope study of selected Hercynian Granitic and surrounding rocks from the Western Carpathians (Slovakia). Geol. Carpathica 53 (1), 3–13.

Krouse, H.R., Coplen, T.B., 1997. Reporting of relative sulfur isotope-ratio data. Pure Appl. Chem. 69 (2), 293–295. https://doi.org/10.1351/pac199769020293.

Kuhn, T., Herzig, P.M., Hannington, M.D., Garbe-Schönberg, D., Stoffers, P., 2003. Origin of fluids and anhydrite precipitation in the sediment-hosted Grimsey hydrothermal field north of Iceland. Chem. Geol. 202, 5–21. https://doi.org/10.1016/S0009-2541(03)00207-9.

Kusakabe, M., Komoda, Y., Takano, B., Abiko, T., 2000. Sulfur isotopic effects in the disproportionation reaction of sulfur dioxide in hydrothermal fluids: implications for the δ34S variations of dissolved bisulfate and elemental sulfur from active crater lakes. J. Volcanol. Geotherm. Res. 97 (1–4), 287–307. https://doi.org/10.1016/S0377-0273(99)00161-4.

Kwon, S., Xie, L., Park, S., Kim, K.I., Min, K.B., Kim, K.Y., Zhuang, L., Choi, J., Kim, H., Lee, T.J., 2019. Characterization of 4.2-km-deep fractured granodiorite cores from Pohang geothermal reservoir, Korea. Rock Mech. Rock Eng. 52, 771–782. https://doi.org/10.1007/s00603-018-1639-2.

Laouar, R., Boyce, A.J., Fallick, A.E., Leake, B.E., 1990. A sulphur isotope study on selected Caledonian granites of Britain and Ireland. Geol. J. 25 (3-4), 359–369. https://doi.org/10.1002/gj.3350250318.

Lawson, M., Polya, D., Boyce, A.J., Bryant, C., Ballentine, C.J., 2016. Tracing organic matter composition and distribution and its role on arsenic release in shallow Cambodian groundwaters. Geochim. Cosmochim. Acta 178, 160–177. https://doi.org/10.1016/j.gca.2016.01.010.

Lee, K.Y., 2017. Hankyoreh online: Scientists discuss correlation between geothermal plant and Pohang earthquake. 27 11. Accessed 2 14, 2018. http://english.hani.co.kr/arti/english_edition/e_national/820906.html.

Lee, S.G., Kim, T.K., Lee, T.J., 2011. Strontium isotope geochemistry and its geochemical implication from hot spring waters in South Korea. J. Volcanol. Geotherm. Res. 208, 12–22. https://doi.org/10.1016/j.jvolgeores.2011.09.004.

Lee, T.-H., Yi, K., Cheong, C.-S., Jeong, Y.-J., Kim, N., Kim, M.J., 2014. SHRIMP U-Pb zircon geochronology and geochemistry of drill cores from the Pohang basin. J. Petrol. Soc. Korea 23 (3), 167–185. https://doi.org/10.7854/JPSK.2014.23.3.167.

Lee, T.J., Song, Y., Park, D.-W., Jeon, J., Yoon, W.S., 2015. Three-dimensional geological model of Pohang EGS pilot site, Korea. In: Proceedings of the World Geothermal Congress. Melbourne, Australia,, 19-25 April 2015. https://pangea.stanford.edu/ERE/db/WGC/papers/WGC/2015/31025.pdf.

Lee, K.-K., Yeo, I.-W., Lee, J.-Y., Kang, T.-S., Rhie, J., Sheen, D.-H., Chang, C., et al., 2019. Summary report of the Korean Government Commission on relations between the 2017. Pohang earthquake and the EGS project. Geological Society of Korea and Korean Government Commission on the Cause of the Pohang Earthquake Pohang earthquake and the EGS project, Seoul, Republic of Korea. Accessed 3 29, 2019. http://www.gskorea.or.kr/custom/27/data/Summary_Report_on_Pohang_Earthquake_March_20_2019.pdf.

Li, P., Zou, H., Hao, F., Yu, X., 2019. Sulfate sources of thermal sulfate reduction (TSR) in the Permian Changxing and Triassic Feixianguan formations, Northeastern Sichuan Basin, China. Geofluids 2019. https://doi.org/10.1155/2019/5898901. Article 5898901.

Machel, H.G., 2001. Bacterial and thermochemical sulfate reduction in diagenetic settings - old and new insights. Sediment. Geol. 140, 143–175. https://doi.org/10.1016/S0037-0738(00)00176-7.

Machel, H.G., Krause, H.R., Sassen, R., 1995. Products and distinguishing criteria of bacterial and thermochemical sulfate reduction. Appl. Geochem. 10 (4), 373–389. https://doi.org/10.1016/0883-2927(95)00008-8.

Miao, Z., Carroll, K.C., Brusseau, M.L., 2013. Characterization and quantification of groundwater sulfate sources at a mining site in an arid climate: the Monument Valley site in Arizona, USA. J. Hydrol. 504, 207–215. https://doi.org/10.1016/j.jhydrol.2013.09.030.

Misstear, B., Banks, D., Clark, L., 2017. Water Wells and Boreholes, 2nd edition. Wiley-Blackwell.

Muramatsu, Y., Komatsu, R., Sawaki, T., Sasaki, M., Yanagiya, S., 2000. Geochemical study of fluid inclusions in anhydrite from the Kakkonda geothermal system, northeast Japan. Geochem. J. 34 (3), 175–193. https://doi.org/10.2343/geochemj.34.175.

Owen, J., Bustin, R.M., Bustin, A.M.M., 2020. Insights from mixing calculations and geochemical modeling of Montney Formation post hydraulic fracturing flowback water chemistry. J. Pet. Sci. Eng. 195 https://doi.org/10.1016/j.petrol.2020.107589. Paper 107589.

Park, K.H., Eastoe, C.J., Choi, S.W., 1991. Ore minerals, fluid inclusions and isotopic (S, C,O) compositions in the diatreme-hosted Nokdong As-Zn deposit, southeastern Korea: the character and evolution of the hydrothermal fluids. J. Korean Inst. Mining Geology 24, 131–150.

Park, J.-Y., Kim, J.-M., Yoon, S.-H., 2015. Three-dimensional geologic modeling of the Pohang Basin in Korea for geologic storage of carbon dioxide. J. Geol. Soc. Korea 51 (3), 289–302. https://doi.org/10.14770/jgsk.2015.51.3.289.

Park, S., Xie, L., Kim, K.-I., Kwon, S., Min, K.-B., Choi, J., Yoon, W.-S., Song, Y., 2017. First hydraulic stimulation in fractured geothermal reservoir. Procedia Eng. 191, 829–837. https://doi.org/10.1016/j.proeng.2017.05.250.

Parkhurst, D.L., C.A.J. Appelo. 2013. "Description of input and examples for PHREEQC version 3: a computer program for speciation, batch-reaction, one-dimensional transport, and inverse geochemical calculations." Chap. A43 in U.S. Geological Survey Techniques and Methods, book 6, 497 pp. Denver, Colorado: United States Geological Survey. https://pubs.usgs.gov/tm/06/a43/.

Richards, J.P., 2011. Magmatic to hydrothermal metal fluxes in convergent and collided margins. Ore Geol. Rev. 40 (1), 1–26. https://doi.org/10.1016/j.oregeorev.2011.05.006.

Rolnick, L.S., 1954. The Stability of Gypsum and Anhydrite in the Geologic Environment. PhD thesis.. Massachusetts Institute of Technology.

Rye, R.O., 2005. A review of the stable-isotope geochemistry of sulfate minerals in selected igneous environments and related hydrothermal systems. Chem. Geol. 215 (1–4), 5–36. https://doi.org/10.1016/j.chemgeo.2004.06.034.

Rye, R.O., Back, W., Hanshaw, B.B., Rightmire, C.T., Pearson, F.J., 1981. The origin and isotopic composition of dissolved sulfide in groundwater from carbonate aquifers in Florida and Texas. Geochim. Cosmochim. Acta 45 (10), 1941–1950. https://doi.org/10.1016/0016-7037(81)90024-7.

Sauty, J.P., 1980. An analysis of hydrodispersive transfer in aquifers. Water Resour. Res. 16 (1), 145–158. https://doi.org/10.1029/WR016i001p00145.

Savage, D., Cave, M.R., Milodowski, A.E., George, I., 1987. Hydrothermal alteration of granite by meteoric fluid: an example from the Carnmenellis Granite, United Kingdom. Contrib. Mineral. Petrol. 96, 391–405. https://doi.org/10.1007/BF00371257.

Seal II, R.R., 2006. Sulfur isotope geochemistry of sulfide minerals. Rev. Mineral. Geochem. 61 (1), 633–677. https://doi.org/10.2138/rmg.2006.61.12.

Stanford University, 2019. Mineral Makeup of Seawater. Accessed 4 12, 2019. https://web.stanford.edu/group/Urchin/mineral.html.

Stober, I., Bucher, K., 1999. Origin of salinity of deep groundwater in crystalline rocks. Terra Nova 11 (4), 181–185. https://doi.org/10.1046/j.1365-3121.1999.00241.x.

Strauss, H., 1997. The isotopic composition of sedimentary sulfur through time. Palaeogeogr. Palaeoclimatol. Palaeoecol. 132, 97–118. https://doi.org/10.1016/S0031-0182(97)00067-9.

Takai, K., Nakamura, K., Toki, T., Tsunogai, U., Miyazaki, M., Miyazaki, J., Hirayama, H., Nakagawa, S., Nunoura, T., Horikoshi, K., 2008. Cell proliferation at 122°C and isotopically heavy CH4 production by a hyperthermophilic methanogen under high-pressure cultivation. Proceedings of the National Academy of Sciences 105 (31), 10949–10954. https://doi.org/10.1073/pnas.0712334105.

Taylor, B.E., Wheeler, M.C., Nordstrom, D.K., 1984. Stable isotope geochemistry of acid mine drainage: Experimental oxidation of pyrite. Geochim. Cosmochim. Acta 48 (12), 2669–2678. https://doi.org/10.1016/0016-7037(84)90315-6.

Tostevin, R., Turchyn, A.V., Farquhar, J., Johnston, D.T., Eldridge, D.L., Bishop, J.K.B., McIlvin, M., 2014. Multiple sulfur isotope constraints on the modern sulfur cycle. Earth Planet. Sci. Lett. 396, 14–21. https://doi.org/10.1016/j.epsl.2014.03.057.

Van Driessche, A.E.S., Stawski, TM, Benning, L.G., Kellermeier, M, 2017. Calcium sulfate precipitation throughout its phase diagram. In: Van Driessche, A., Kellermeier, M., Benning, L., Gebauer, D. (Eds.), New perspectives on mineral nucleation and growth. Springer Nature Switzerland AG, Cham, Switzerland, pp. 227–256. https://doi.org/10.1007/978-3-319-45669-0_12.

Vazquez, O., Mehta, R., Mackay, E.J., Linares-Samaniego, S., Jordan, M.M., Fidoe, J., 2014. Post-frac flowback water chemistry matching in a shale development. SPE International Oilfield Scale Conference and Exhibition. Society of Petroleum Engineers, Aberdeen, Scotland. https://doi.org/10.2118/169799-MS.

Vidal, J., Patrier, P., Genter, A., Beaufort, D., Dezayes, C., Glaas, C., Lerouge, C., Sanjuan, D., 2018. Clay minerals related to the circulation of geothermal fluids in boreholes at Rittershoffen (Alsace, France). J. Volcanol. Geotherm. Res. 349, 192–204. https://doi.org/10.1016/j.jvolgeores.2017.10.019.

Westaway, R., Burnside, N., 2019. Fault 'corrosion' by fluid injection: a potential cause of the November 2017 Mw 5.5 Korean earthquake. Geofluids. https://doi.org/10.1155/2019/1280721. Article ID 1280721.

Westaway, R., Burnside, N.M., Banks, D., 2020. Hydrochemistry of produced water from the Pohang EGS project site, Korea: implications for water-rock reactions and associated changes to the state of stress accompanying hydraulic fracturing of granite. In: Proc. World Geothermal Congress 2020 (April 26th-May 2nd 2020). Reykjavik, Iceland. https://pangea.stanford.edu/ERE/db/WGC/papers/WGC/2020/15037.pdf.

Winkel, B.J., 1994. Modelling mixing problems with differential equations gives rise to interesting questions. Int. J. Mathematical Education Sci. Technol. 25 (1), 55–60. https://doi.org/10.1080/0020739940250107.

Xing, W., Yin, M., Lv, Q., Hu, Y., Liu, C., Zhang, J., 2014. 1 - Oxygen solubility, diffusion coefficient, and solution viscosity. In: Xing, W., Yin, G., Zhang, J. (Eds.), Rotating electrode methods and oxygen reduction electrocatalysts, pp. 1–31. https://doi.org/10.1016/B978-0-444-63278-4.00001-X. Elsevier B.V.

Yoon, C.H., Jung, H.S., 2008. Gold abundance and stable isotopes (H, O, S) in hydrothermal alteration zones of Gasa Island (Gasado), Korea. Resour. Geol. 58 (1, 87–99. https://doi.org/10.1111/j.1751-3928.2007.00046.x.

Yoon, K.-S., Jeon, J.-S., Hong, H.-K., Kim, H.-G., Hakan, A., Park, J.-H., Yoon, W.-S., 2015. Deep drilling experience for Pohang enhanced geothermal project in Korea. In: Proceedings World Geothermal Congress, Melbourne, Australia, 19-25 April 2015. Melbourne, Australia. https://pangea.stanford.edu/ERE/db/WGC/papers/WGC/2015/06034.pdf.

Zarrouk, S.J., McLean, K., 2019. Chapter 9 - Operation and management of geothermal wells. In: Zarrouk, S.J., McLean, K. (Eds.), Geothermal well test analysis: fundamentals, applications and advanced techniques. Elsevier BV, pp. 217–255. https://doi.org/10.1016/B978-0-12-814946-1.00009-8.

Zastrow, M., 2019. South Korea Accepts Geothermal Plant Probably Caused Destructive Quake. Nature News (online). https://doi.org/10.1038/d41586-019-00959-4.

Zolfaghari, A., Tang, Y., Holyk, J., Binazadeh, M., Dehghanpour, H., Bearinger, D., 2015. Chemical analysis of flowback water and downhole gas-shale samples. In: SPE/CSUR Unconventional Resources Conference. Calgary, Canada: Society of Petroleum Engineers. https://doi.org/10.2118/175925-MS.